NASA Technical Memorandum 108992
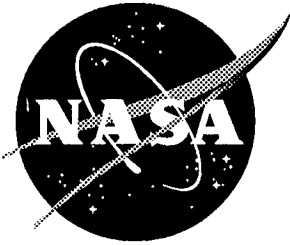
Test and Analysis of a Stitched RFI Graphite-Epoxy Panel with a Fuel Access Door

Dawn C. Jegley
Langley Research Center, Hampton, VA

W. Allen Waters, Jr.
Lockheed Engineering and Sciences Company, Hampton, VA

March 1994

TEST AND ANALYSIS OF A STITCHED RFI GRAPHITE-EPOXY PANEL

WITH A FUEL ACCESS DOOR

Dawn C. Jegley and W. Allen Waters, Jr.

Abstract

A stitched Resin-Fusion-Injection (RFI) graphite-epoxy panel with a fuel access door was analyzed using a finite element code and was loaded to failure in compression. The panel was subjected to low-speed impact damage by an impactor with impact energy of 100 ft-lb prior to compressive loading. The impact damage was not detectable visually or by A-scan inspection. The panel failed at an applied load of 695,000 lb and a global failure strain of .00494 in/in. Analysis predicts that the panel would fail due to collapse at a load of 688,100 lb. The test data indicate that the maximum strain occurs in a region near the access door and was .0096 in/in. Analysis indicates that this local surface strain is .010 in/in at the panel's failure load. The panel did not fail through the impact-damage site, but instead failed through bolt holes used to attach the access door to the panel. The bolt holes are in a region of high strain.

Introduction

In an attempt to make viable the use of composite materials for aircraft primary structures, methods of fabrication and manufacturing involving non-traditional material forms are being explored. Composite materials will not

be used extensively for transport primary structure unless cost-effective, structurally efficient and reliable composite parts can be fabricated. The NASA Langley Research Center and several contractors are developing new concepts for achieving this goal (see refs. 1-3). One material form and associated manufacturing method which may prove to meet these criteria are stitched panels fabricated using the Resin-Fusion-Injection (RFI) fabrication process. The stitching may reduce the incidence of delaminations and reinforce the bond between stiffeners and skin without the use of mechanical fasteners. The RFI process is a relatively low-cost manufacturing method which can be used to fabricate stiffened panels (ref. 4).

To explore the potential of stitched RFI panels, Douglas Aircraft Company designed and constructed a wing compression panel with a fuel access door. The panel is designed to model the behavior of an upper wing-skin cover panel of a transport aircraft. The effect of impact damage, bolt holes and the panel's structural stability have been examined. This panel was delivered to NASA Langley Research Center for compression testing. Initial analyses and testing were conducted by Douglas (ref. 5). Final analysis and testing were conducted at NASA Langley Research Center and the results of this work are presented in this report.

Test Specimen

The panel is 56 inches long, 36.75 inches wide and has two intercostals and four stringers as shown in figure 1. The skin, flanges and blade stiffeners

of the panel were constructed from Hercules, Inc. AS4/3501-6 graphite-epoxy material with a skin and blade stacking sequence of $[0/45/0/-45/90/-45/0/45/0]_8$ and a stringer flange stacking sequence of $[0/45/0/-45/90/-45/0/45/0]_4$. The panel was fabricated by first stitching the dry preform and then infusing the resin into the preform using a resin-fusion-injection process. The skin, blades and flanges were stitched and then cocured. No mechanical fasteners were used to attach the flanges to the skin. The land ring for the access door was constructed from graphite-epoxy material and was used to attach the door to the panel skin. The access door was a sandwich construction with a Rohacell foam core and E-glass/epoxy face sheets. The access door is oval and is located in the center of the panel. It is 18 inches long and 15 inches wide. Thirty-six .25-inch-diameter bolts were used to attach the door to the land ring and thirty-six .3125-inch-diameter bolts were used to attach the land ring to the panel skin.

Prior to testing, the ends of the panel were potted in an epoxy compound and machined flat and parallel. The panel skin was impacted at two locations with 100 foot-pounds of impact energy using a dropped-weight impactor. The impact sites were .75 inches below the panel centerline and .5 inches outboard of each side of the access door, as shown in figure 1. The impacts caused no visible damage and no damage was detectable by A-scan inspection.

Photographs of the stiffened side of the panel, the unstiffened side of the panel and the cross section of the test specimen are shown in figures 2, 3 and 4, respectively. Both the stiffened and unstiffened sides of the panel were

painted white prior to testing to improve the quality of photographs and to allow the use of moire interferometry during the test.

A total of 76 strain gages were bonded to the panel using the pattern shown in figure 5(a). Back-to-back strain gages were placed on the skin, stringers, door and land ring. Nine Direct Current Differential Transformers (DCDT's) were used to measure panel displacements and their locations are shown in figure 5(b).

The panel was loaded in axial compression up to 500,000 lb by the Douglas Aircraft Company prior to delivery to NASA Langley Research Center. No evidence of failure or damage was detected during this preliminary test.

The test apparatus at NASA Langley Research Center consisted of a panel restraint fixture and the Langley 1.2-million-pound-capacity hydraulic test machine. The restraint fixture was designed to prevent out-of-plane motion at the intercostals while allowing the panel to shorten when load was applied. A drawing of the restraint fixture is shown in figure 6. The panel was loaded to failure at a rate of 100,000 lb/min up to a load of 400,000 lb and a rate of 50,000 lb/min from 400,000 lb to failure. Data were recorded from all gages and DCDT's throughout the test. The behavior of the unstiffened side of the access door panel during loading was monitored by using moire interferometry to exhibit out-of-plane deformations. These resulting out-of-plane deformation patterns were photographed using still photography at various load levels and were recorded on video tape. The behavior of the panel's stiffened side was also recorded on video tape.

Analysis

An initial analysis was conducted using the finite element code NASTRAN (ref. 6) to predict panel behavior. Results of the NASTRAN analytical study are presented in reference 5 and indicate that the panel would not buckle prior to failure, that the bolts would not fail in shear and that the bearing stress in the panel skin at the bolt locations would not induce a premature failure. Failure was predicted to be in the region of high strain near the cutout for the access door and through an impact site. In addition, a detailed discussion of the effect of the impact on the panel behavior is presented in reference 5. Detailed results of the NASTRAN analysis are not presented herein.

In the present study, the finite element code STAGS (reference 7) was used to predict panel behavior. The model used in the STAGS analysis is shown in figure 7. Beam, triangular plate and quadrilateral plate elements were used to model one quarter of the panel. A total of 604 nodes and 3720 degrees of freedom were used in the model. Symmetry conditions were assumed on two edges of the model, as shown in the figure. The loaded ends of the panel were assumed to be clamped and the unloaded edges were assumed to be free. The potting material at the ends of the panel was not considered in the model. Out-of-plane motion was not permitted at the top of the intercostals due to the presence of the restraint fixture. Any effect of the impact damage was neglected in the analysis.

Since out-of-plane motion occurs in the panel (prior to buckling), a nonlinear analysis was used. Two STAGS analyses were conducted for a comparison with test data. Nominal linear material properties were assumed in all parts of the panel in the first analysis. However, since coupon test results reported in reference 8 indicate that the stitched graphite-epoxy material behaves nonlinearly, an analysis using nonlinear material properties for the skin, flanges and blades was also conducted. Assumed linear material properties for the stitched graphite-epoxy skin, blade and flange material, land ring material and access door materials are shown in table I. Assumed nonlinear behavior based on the coupon tests, in the form of a stress-strain relationship for the stitched graphite-epoxy material, is shown in table II.

A buckling analysis was also conducted, using STAGS, to verify that buckling would not occur at a load less than the panel failure load. An analysis of the buckling load was conducted based on a nonlinear prebuckling stress state and nonlinear material properties.

Results and Discussion

The panel sustained a maximum compressive load of 695,000 lb, P_{max}, before failure, resulting in a maximum stress resultant, N_x, of 18,912 lb/in. Significant out-of-plane deformations occurred as the panel was loaded due to the eccentricities of the door, land ring and stiffeners. As the loading increased, the out-of-plane deformation increased. Photographs showing the out-of-plane deformation patterns of the unstiffened skin and access door are

6

shown in figure 8 for load levels, P, of 210,000 lb (P/P_{max} = .30), 396,000 lb (P/P_{max} = .57), 591,000 lb (P/P_{max} = .85) and 671,000 lb (P/P_{max} = .97). These moire patterns show the overall progression of the out-of-plane deformation during loading.

The maximum load level considered in the nonlinear analysis with linear properties is 700,000 lb which is approximately the load at which the panel failed. No buckling or collapse was indicated prior to this load level for the analysis with linear properties. However, in the analysis with nonlinear properties, the maximum load considered was 688,160 lb because panel collapse was predicted at approximately this load level. Analysis also indicates the presence of significant out-of-plane deformations at low load levels and of large deformations as the panel approached failure. A contour plot of the out-of-plane deformations calculated using finite elements with assumed nonlinear material properties at a load level of 688,160 lb is shown in figure 9. The buckling calculation indicates that the minimum buckling load of the panel is 1,046,000 lb. This value is well above the panel failure load so buckling would not influence the behavior of the panel.

The photographs and the recorded deformations indicate that out-of-plane deformation of the access door occurred almost from the onset of loading. Deformations of the skin above the top intercostal and below the bottom intercostal did not occur until a load of approximately 550,000 lb was reached. The contour plot indicates the presence of large out-of-plane deformations in the access door and smaller out-of-plane deformations near the potted ends.

7

Measured end-shortening of the panel during loading at approximately the lateral centerline of the panel indicates that there was no significant change in global stiffness prior to a load of approximately 85 percent of the failure load. In the load range within 10 percent of the failure load, the global stiffness is reduced by 40 percent compared to the initial global stiffness. This result and the end-shortening predicted by finite element analysis using linear and nonlinear material properties are shown in figure 10. The analysis using linear material properties results in an initial global stiffness 11 percent higher than the measured stiffness of the panel, while the analysis using nonlinear properties results in an initial global stiffness .7 percent higher than the measured stiffness of the panel.

The maximum global axial strain can be determined from the failure (or maximum) load divided by the panel length. This calculation results in an experimental global strain of .00494 in/in at failure. Analysis using linear material properties indicates that at a load of 700,000 lb, the global strain is .00417 in/in (15 percent lower than the experimentally determined failure strain) and analysis using nonlinear properties indicates that collapse would occur at 688,160 lb with a global strain of .004601 in/in. Comparing the collapse conditions with the experimental conditions at failure indicates that the analytical global failure strain is 7 percent lower than the experimental failure strain but the analytical failure load is 1 percent lower than the experimental failure load. Since panel stiffness was not exactly the same in the test as in the analysis, the percentage difference between experimental and analytical failure loads is not the same as the percentage difference between experimental and analytical failure strains.

A sketch of the deformations showing the end-shortening and out-of-plane deformations is shown in figure 11. The locations of the lateral support frame and the intercostals of the panel are shown. Prior to loading, an aluminum plate approximately one inch square was bonded to the top of the rib of each intercostal perpendicular to the rib and near the lateral center, so out-of-plane deformation measurements could be taken. As the panel shortens, the loaded ends and the intercostals do not move out-of-plane. All other parts of the panel except the potted ends do move out-of-plane. The intercostals move downward as the panel shortens. As the skin and stringers deform out-of-plane, the intercostal ribs are forced to rotate, as shown in the figure. The motion of the intercostal ribs was monitored by one DCDT on the top intercostal and another DCDT on the bottom intercostal measuring the out-of-plane motion of the aluminum plate bonded to the end of the intercostal rib. As the rib rotates, the aluminum plate also rotates. The measurement location remains unchanged relative the test machine, but since the panel shortens, the measurement locations change relative to the intercostal ribs. Therefore, this measurement is an accurate measure of the out-of-plane deformation until rib (and plate) rotation begins. DCDT measurements at the intercostal ribs are shown in figure 12. These results indicate that the ribs begin to rotate at a load of approximately 400,000 lb. Prior to that load level, the results indicate that no out-of-plane intercostal rib deformation takes place. Since the end-shortening and intercostal deformation plots are smooth curves and no damage to the connection pins through the intercostal ribs was visible after the test, the assumption is made that no binding occurred as the ribs rotated.

9

Four DCDT's measured out-of-plane motion along the axial centerline of the panel, as shown in figure 5(b). These measurements are shown in figure 13 and indicate that out-of-plane deformations take place at very low load levels. At failure, the center of the access door has moved out-of-plane almost .8 inches. The skin next to the access door has moved approximately .6 inches. The maximum deformation at midbay between the stringers is only .3 inches and the panel edge has moved .15 inches. The deformations at these locations predicted by finite element analysis are also shown in figure 13. The analysis with linear material properties consistently predicts significantly lower deformations than those measured. The analysis with nonlinear material properties predicts deformations with the same trend in deformation as the measurements and predicts more accurate deformations at failure than the analysis with linear material properties.

A measurement of the motion in the lateral direction of one of the outermost stringers representing the rotation due to rolling of the stringer is shown in figure 14. Calculated motion representing rolling of the stringer is also shown in the figure. This measurement indicates that rolling occurred from the onset of loading. Analysis using linear material properties shows the correct trend but not the correct displacement values. Analysis using nonlinear material properties accurately predicts this motion.

Strain gages were located far from the access door to determine whether the load introduction was constant across the width of the panel. Strains recorded by back-to-back strain gages on the top of the outermost stringers and the opposite skin are shown in figure 15(a). These strain gages indicate

10

uniform load introduction occurred until this region of the panel started to bend at about 400,000 lb. After bending initiated, the back-to-back strain gages on the stringers and the skin no longer recorded the same strain. Strain gages were also placed far from the access door on the lateral centerline to monitor bending in the skin above the top intercostal and below the bottom intercostal. Strains recorded by these strain gages are shown in figure 15(b). Predicted strains at these locations are also shown in the figure. Significant bending takes place in the panel skin for loads above about 200,000 lb. Predicted strains from analysis using nonlinear material properties agree with the test data.

A series of back-to-back axial strain gages was placed along the panel centerline. Strain gages were placed on the skin, stringers, land ring and access door, as shown in figure 5(a). The experimental results and the finite element predictions of surface strains at these locations are shown in figures 16-20. Results for strain gages located one inch from the edge of the panel are shown in figure 16. Results for strain gages located midway between the stringers are shown in figure 17. Results for strain gages located on the skin at the edge of the cutout for the access door are shown in figure 18. Results for strain gages on the land ring back-to-back with the strain gage on the skin of the stiffened side at the cutout for the access door are shown in figure 19. Results for back-to-back axial strain gages on the stringers are shown in figure 20. Results for a pair of strain gages near the tops of the innermost stringers and the skin beneath them are shown in figure 21. Strains for the stringer closest to the access door used to evaluate rolling of the stringer are shown in figure 22. Strain gage rosettes were placed on the skin

4 inches above the bottom intercostal. Measured and calculated strains at this location are shown in figure 23. Axial strain is shown in figure 23(a) and lateral strain is shown in figure 23(b).

These results indicate that more strain and more deformation occurs in the stringers closest to the access door than in the outboard stringers and that significant nonlinear behavior occurs. Finite element analysis using nonlinear material properties accurately predicts all the trends of the strains at these locations and agrees well with the actual experimental results in most cases. Analysis indicates a maximum surface strain of .01 in/in and the maximum experimentally measured strain is .0096 in/in. The difference in strains for the back-to-back strain gages on the stringer oriented normal to the skin indicates that rolling occurs above approximately 300,000 lbs of load.

A contour plot of the axial strain predicted by the analysis at a load of 688,160 lb using nonlinear material properties is shown in figure 24. The region of highest axial strain is near midlength and between the innermost stringer and the cutout for the access door.

The panel failed at a load of 695,000 lb in an overall collapse mode. The damage induced at collapse involved initial failures across the width at approximately 2 inches below midlength on the skin on one side of the access door and approximately 3 inches below midlength on the skin on the other side of the door. The failure passes through the bolt holes on both sides of the access door. This region has the highest axial strain, as shown in figure 24.

Photographs of the stiffened and unstiffened sides of the panel after failure are shown in figure 25(a) and (b), respectively. Failures near midlength and near the intercostals can be seen. The failures at the intercostals occurred after the midlength failures. All four stringers failed from the top of the blade to the skin, as shown for one of the outermost stringers in figure 25(c). The stitched flanges did not separate from the skin at any location.

The failure does not pass through the impact site (which is located .75 inches below the midlength location and .5 inches from the edge of the cutout for the door) on either side of the door. Photographs of the failure and impact sites are shown in figure 26.

Since the panel failed through bolt holes in a region of high strain, a comparison with results of filled-hole compression tests using coupons made from a material similar to that used to construct the graphite-epoxy parts of the access door panel may be useful. In the study presented in ref. 8, filled bolt holes reduced the strength of the unstitched coupons to 78.5 percent of their unnotched strength while filled bolt holes reduced the strength of the stitched coupons to 81.7 percent of their unnotched strength. Using the ultimate stress for the graphite-epoxy material in the access door panel of 98.5 ksi (ref. 8) and these reductions in strength values, predictions of local failure strain can be calculated. By assuming the nonlinear stress-strain relationship presented in table II, the predicted failure strain is between .00975 in/in and .0102 in/in, which differs from the maximum measured surface strain of .0096 in/in by about 1 to 6 percent. By assuming a linear stress-strain relationship, the predicted failure strain is between .0084

13

in/in and .00877 in/in, which differs from the measured strain by 9 to 14 percent. Therefore, nonlinear material properties more accurately predict the maximum strain at failure.

In addition, the panel failed at the top and bottom intercostals after the initial failure through the bolt holes and access door. Sections of the intercostals completely separated from the skin and the skin cracked across the entire width at the bottom intercostal and from the edge of the panel to the innermost stringer on each side at the top intercostal. The failures at the bottom intercostal can be seen in figure 25(b).

Concluding Remarks

A graphite-epoxy panel with a stitched skin with a fuel access door was fabricated using the resin-fusion-injection (RFI) process. This RFI compression panel sustained a load of 695,000 lb and .0049 in/in axial strain before failing. A geometrically nonlinear finite element analysis using nonlinear material properties for the stitched graphite-epoxy material was used to study panel behavior. Nonlinear analysis using nonlinear material properties was necessary to correlate with experimental results. Predictions of overall stability of the panel and local strains must be accurate in the region of loading when the panel behaves nonlinearly to have good agreement with test results. Accuracy of local strains near the access door, near the access-door bolt holes and in the stringers near the access door are of particular importance.

The behavior of the panel as the compressive load was applied is outlined as follows. Significant out-of-plane deformations occurred at low load levels in the region of the panel between intercostals. Bending of the panel skin began at a load of 200,000 lb. The outermost stiffeners began to roll at a load of approximately 300,000 lbs. Uniform load introduction occurred until a load of 400,000 lb was reached, when the intercostal ribs begin to rotate. Out-of-plane deformations of the skin above the top intercostal and below the bottom intercostal began at a load of approximately 550,000 lb. There was no significant change in global stiffness prior to a load of approximately 600,000 lb. In the load range between 600,000 and 690,000 lb, the global stiffness was reduced by 40 percent compared to the initial global stiffness and large deformations occurred as the panel approached failure. The panel failed at a load of 695,000 lb in an overall collapse mode.

The maximum local strain was approximately .0096 in/in and the panel failed through bolt holes used for attaching the access door to the panel. This result is in good agreement with results from coupon tests for specimens with filled bolt holes. Impact with 100 ft-lb of impact energy prior to compressive loading in a region of high axial strain did not cause enough damage to induce failure at the impact site. The panel behavior was predicted accurately. The stitched flanges did not separate from the skin at any location.

References

1. Davis, J.: Advanced Composites Technology Program. Presented at the Third NASA Advanced Composites Technology Conference, Long Beach, California, 1992. NASA CP 3178, 1992, pp. 49-78.

2. Kinder, R.: Impact of Composites on Future Transport Aircraft. Presented at the Third NASA Advanced Composites Technology Conference, Long Beach, California, 1992. NASA CP 3178, 1992, pp. 3-24.

3. Chen, V.; Hawley, A.; Klotzsche, M.; Markus, A.; and Palmer, R.: Composites Technology for Transport Primary Structure. Presented at the First NASA Advanced Composites Technology Conference, Seattle, Washington, 1990. NASA CP 3104, 1991, pp. 71-126.

4. Markus, A.: Resin Transfer Molding for Advanced Composite Primary Wing and Fuselage Structures. Presented at the Second NASA Advanced Composites Technology Conference, Lake Tahoe, Nevada, 1991. NASA CP 3154, 1992, pp. 141-167.

5. Anon.: ICAPS Phase B Access Door Subcomponent Strength Prediction. Douglas Aircraft Company Report MDC-92K0352, February, 1993.

6. Reymond, M., editor: MSC/NASTRAN Version 67 User's Manual, The MacNeal-Schwendler Corporation, 1991.

7. Almroth, B. O.; and Brogan, F. A.: The STAGS Computer Code. NASA CR-2950, February 1978.

8. Hinrichs, S.C.: ICAPS Composite Wing 7-Ply Searbeck and Heinsco Coupon Test Results. McDonnell Douglas Aerospace Transport Aircraft Report No. MDC93K0365, 1993.

Table I. Linear Material Properties

	Section of panel			
	Skin, blades (72 plies)	Land ring (20 plies)	Door skin (20 plies)	Door foam
Stiffness, E_{11}, ksi	9.178×10^3	7.881×10^3	2.955×10^3	9.548
Stiffness, E_{22}, ksi	4.520×10^3	7.881×10^3	2.995×10^3	9.548
Shear Stiffness, G_{12}, ksi	2.334×10^3	3.010×10^3	1.074×10^3	3.548
Poisson's ratio, v_{12}	.4209	.3090	.2257	.3455

Table II. Nonlinear Stress—Strain Data for Skin, Stringers and Ribs

Strain, in/in	Stress, psi
0.	0.
.001	9060.
.002	17,656.
.004	34,384.
.006	50,184.
.008	65,056.
.010	79,000.
.012	92,016.
.014	104,104.

Figure 1. Access door panel geometry and impact sites. All dimensions are in inches.

Land ring

Access door
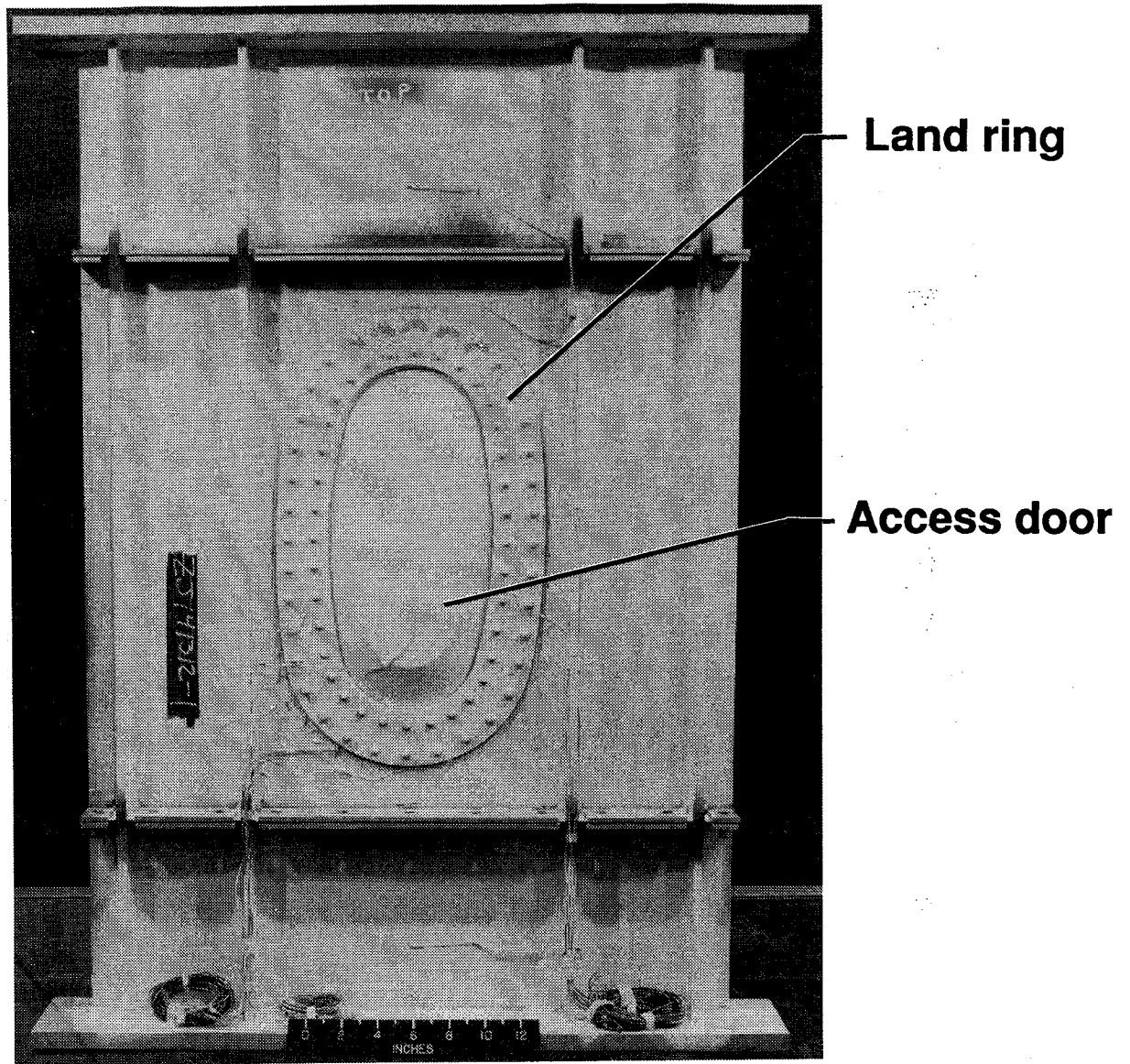
Figure 2. Stiffened side of test specimen prior to test.
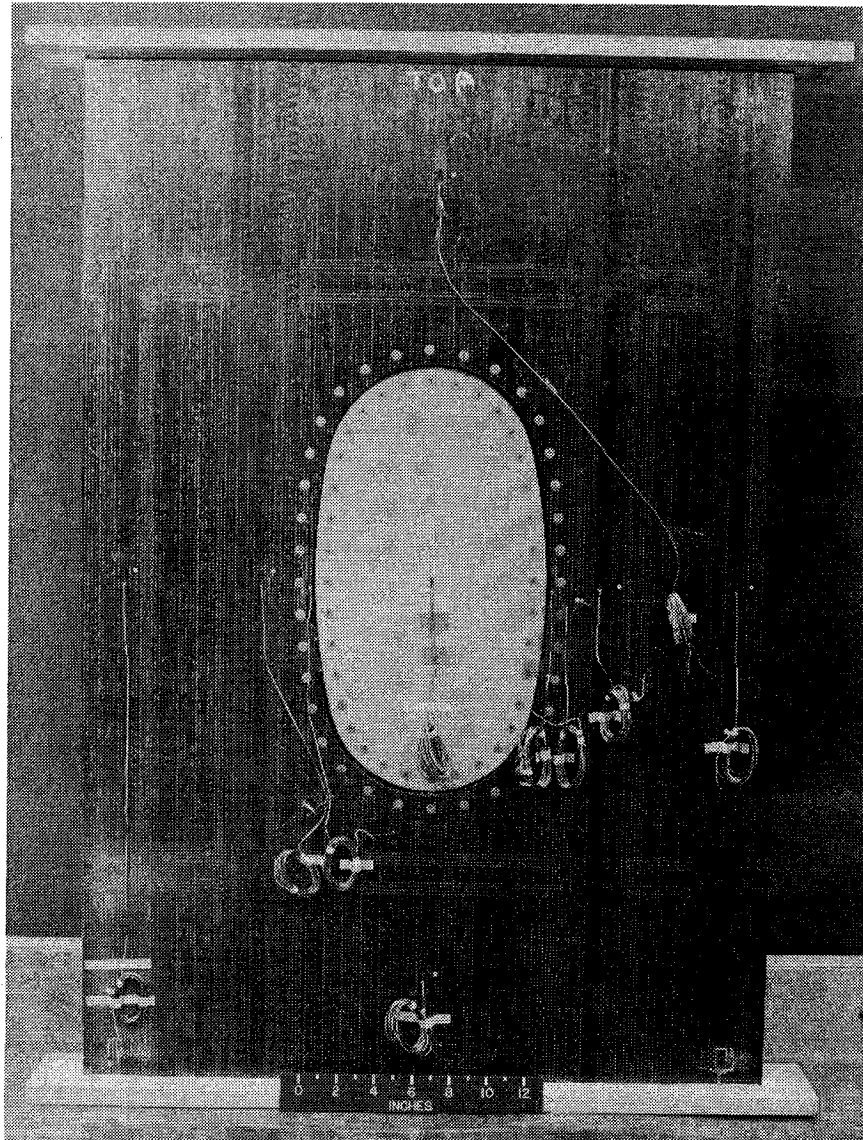
Figure 3. Unstiffened side of test specimen prior to test.

Potting compound

Graphite-epoxy panel
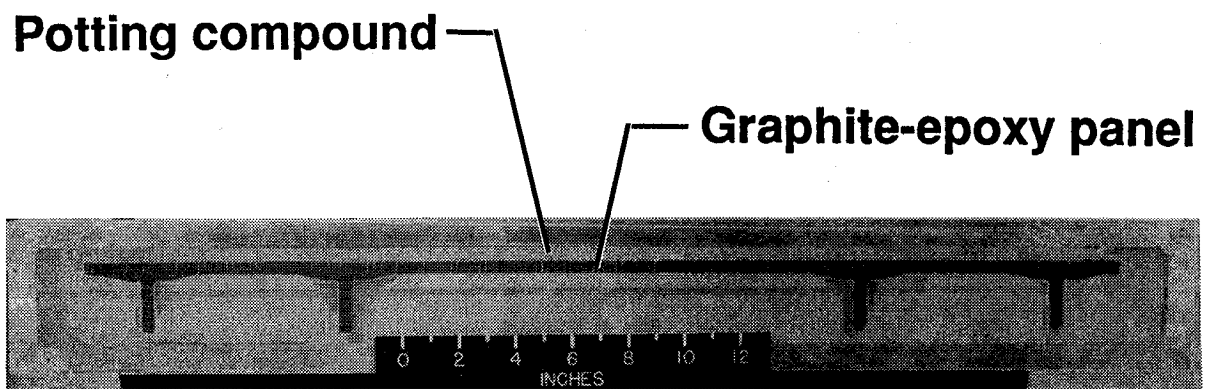
Figure 4.   Cross-sectional view of test specimen.

Rib

Access door

Rib

Potting

Land ring
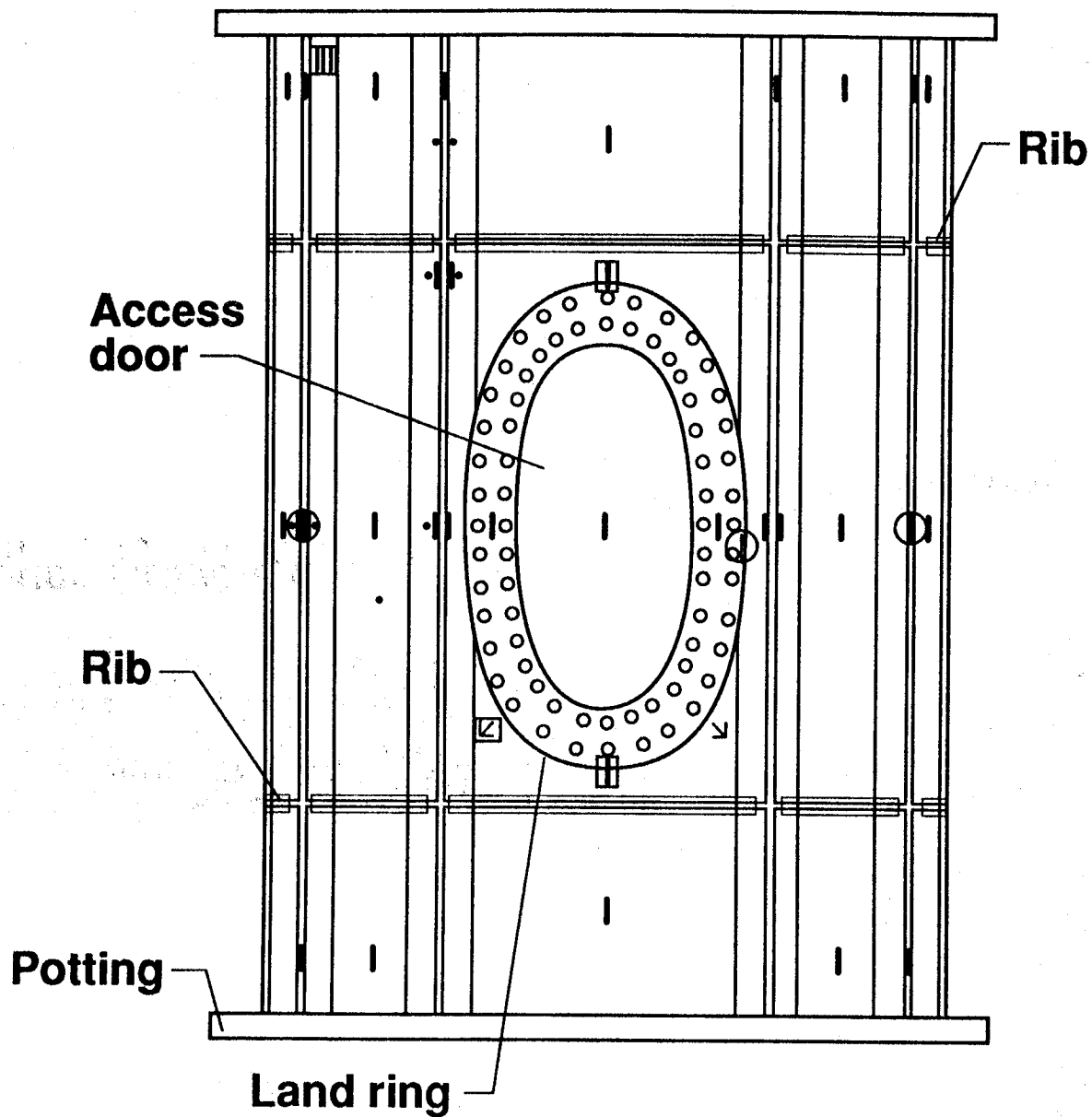
⬚ Axial strain gage on stiffened side only
⬚ Axial strain gage on unstiffened side only
| Back-to-back axial strain gages
⬚ Rosette on stiffened side only
↘ Back-to-back rosettes
• Stiffener strain gages normal to skin
o Bolt

5(a). Strain gage pattern.

**DCDT'S measuring
out-of-plane deformation**

**DCDT'S measuring
axial deformation**

DCDT'S measuring stiffener rolling

2.0

1.0

0.5

2.0

$\mathbb{C}_L$

$\mathbb{C}_L$
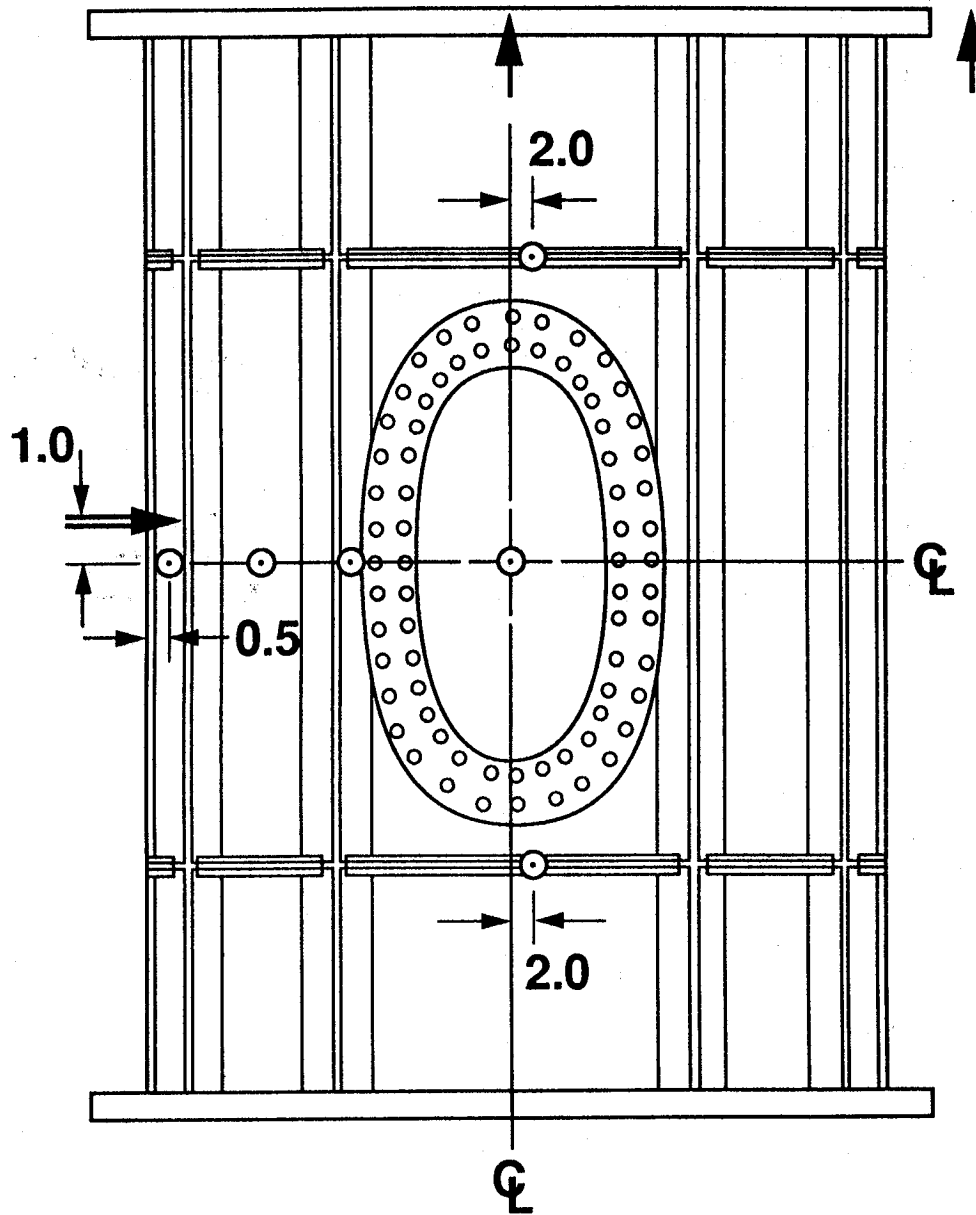
5(b). Locations of displacement measurements.

Figure 5. Strain gage and DCDT locations. All dimensions are in inches.
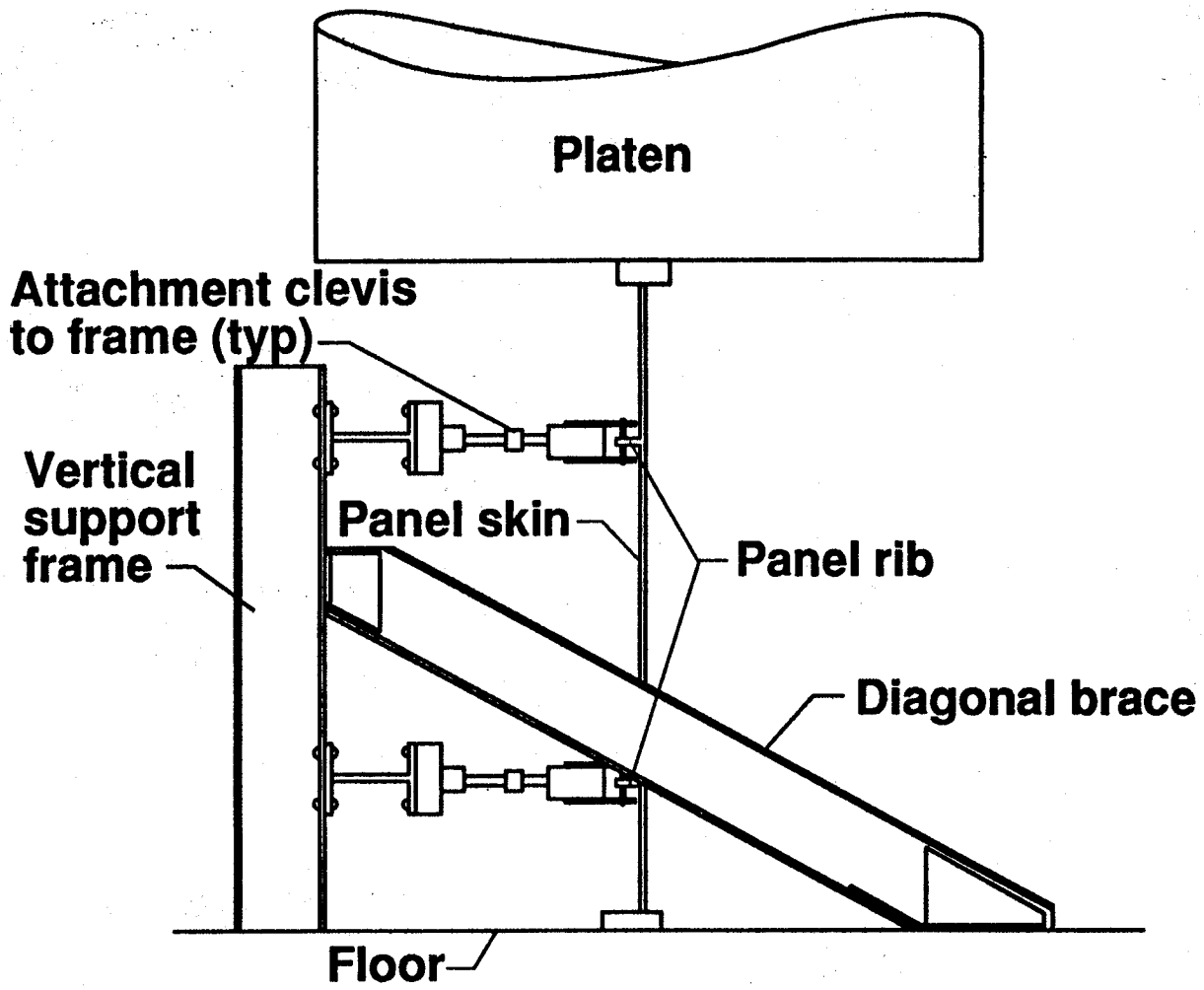
Figure 6. Experimental apparatus and restraint fixture.

Clamped edge

Loading direction

Stringers

Rib

Symmetry along edge

Door

Land ring

z,w

y,v

x,u

Free edge

Symmetry along edge
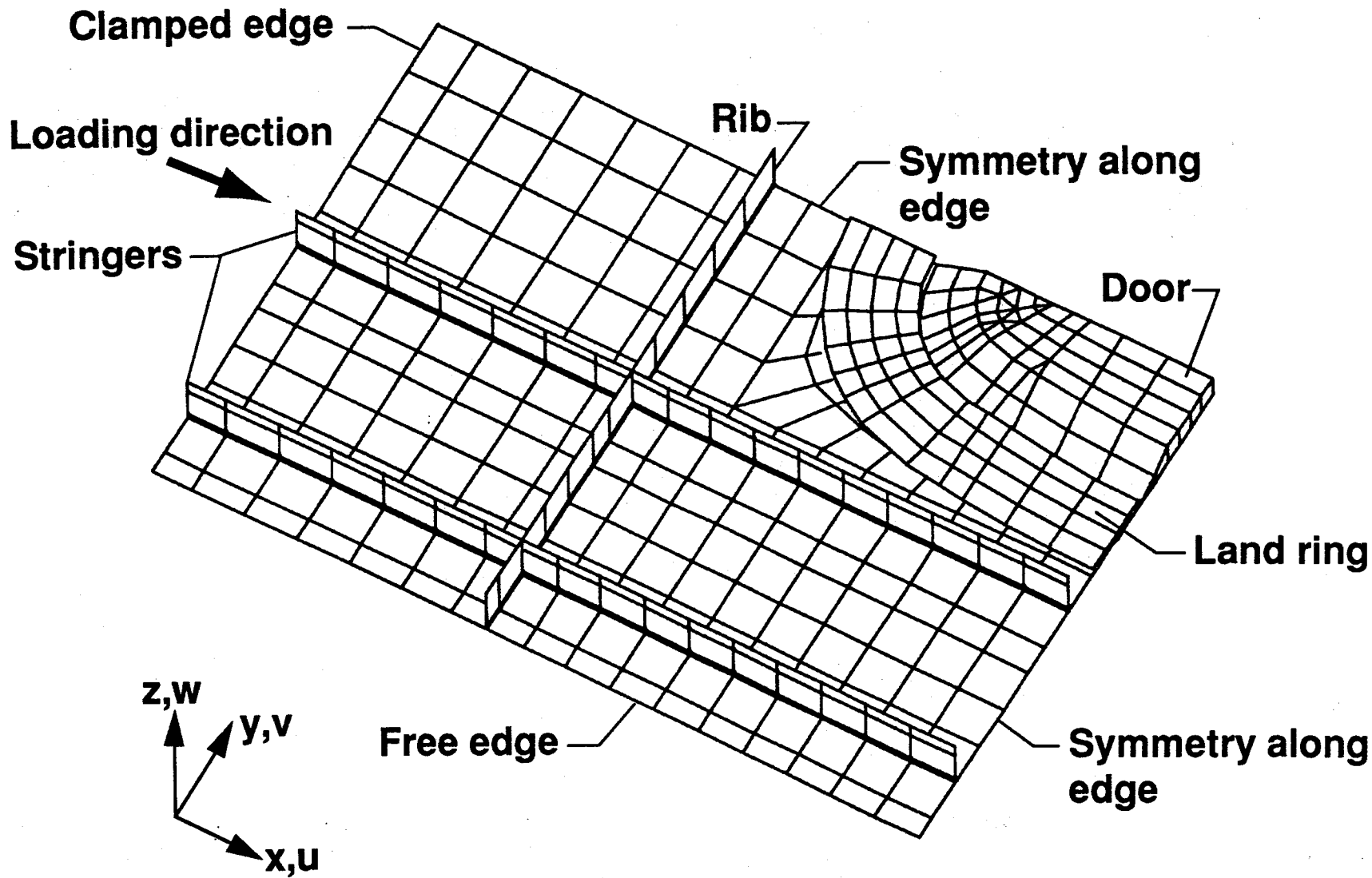
Figure 7.   Finite element model.
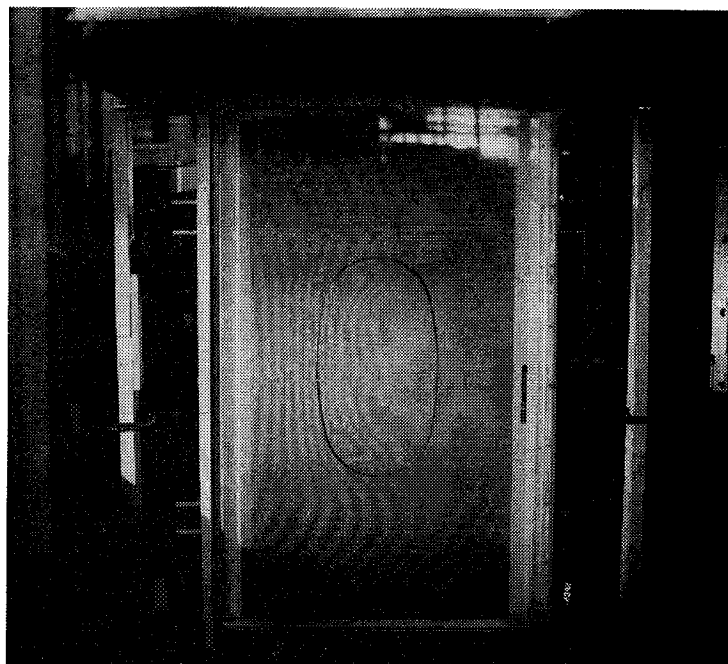
(a) P=210,000 lb (P/P$_{max}$=.30).
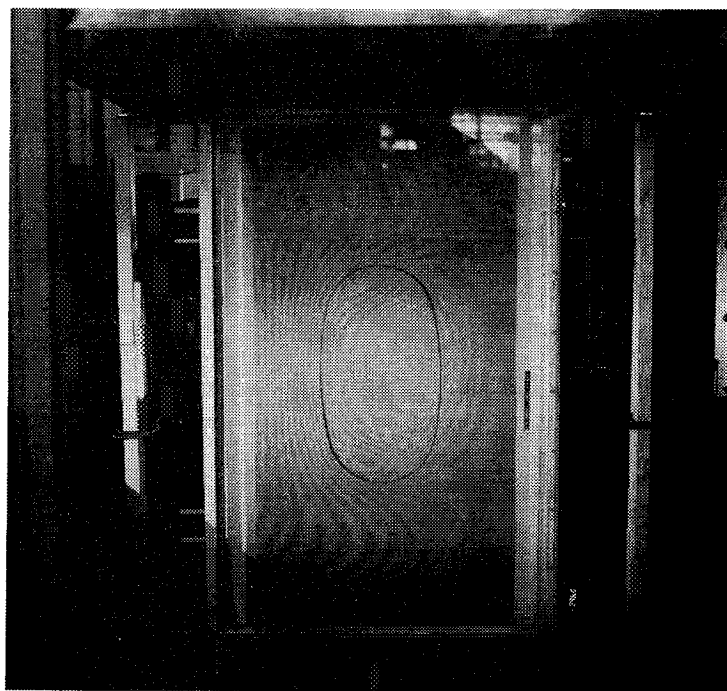
(b) P=396,000 lb (P/P$_{max}$=.57).
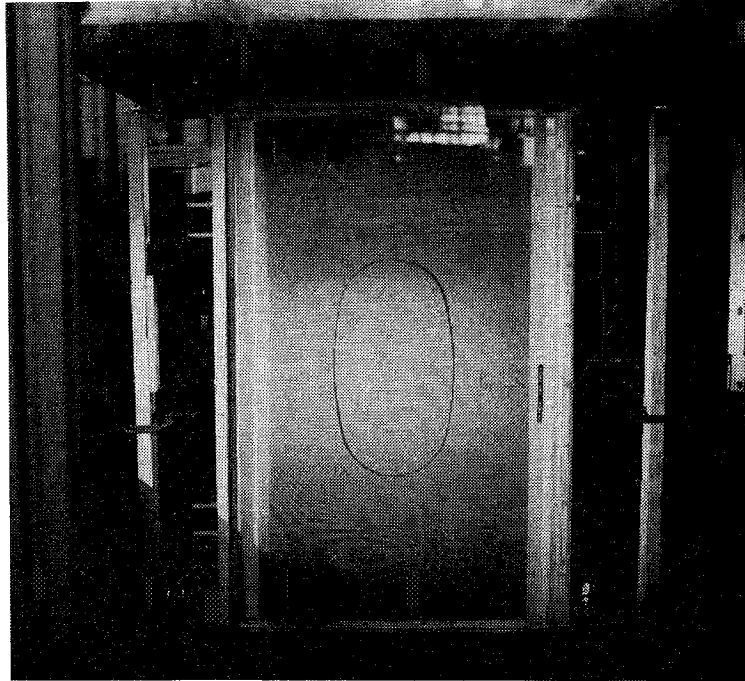
(c) P=591,000 lb (P/P$_{max}$=.85).
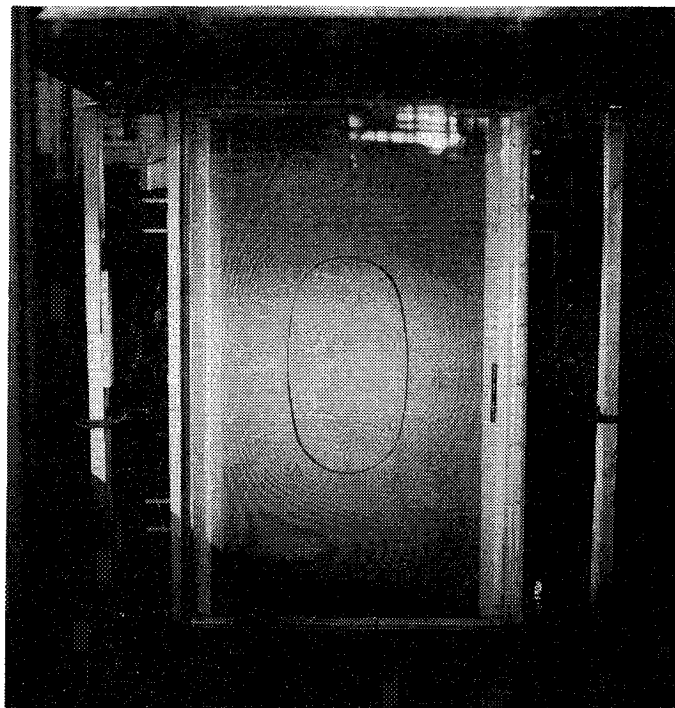
(d) P=671,000 lb (P/P$_{max}$=.97).

Figure 8. Out-of-plane deformation patterns of panel during loading.

27
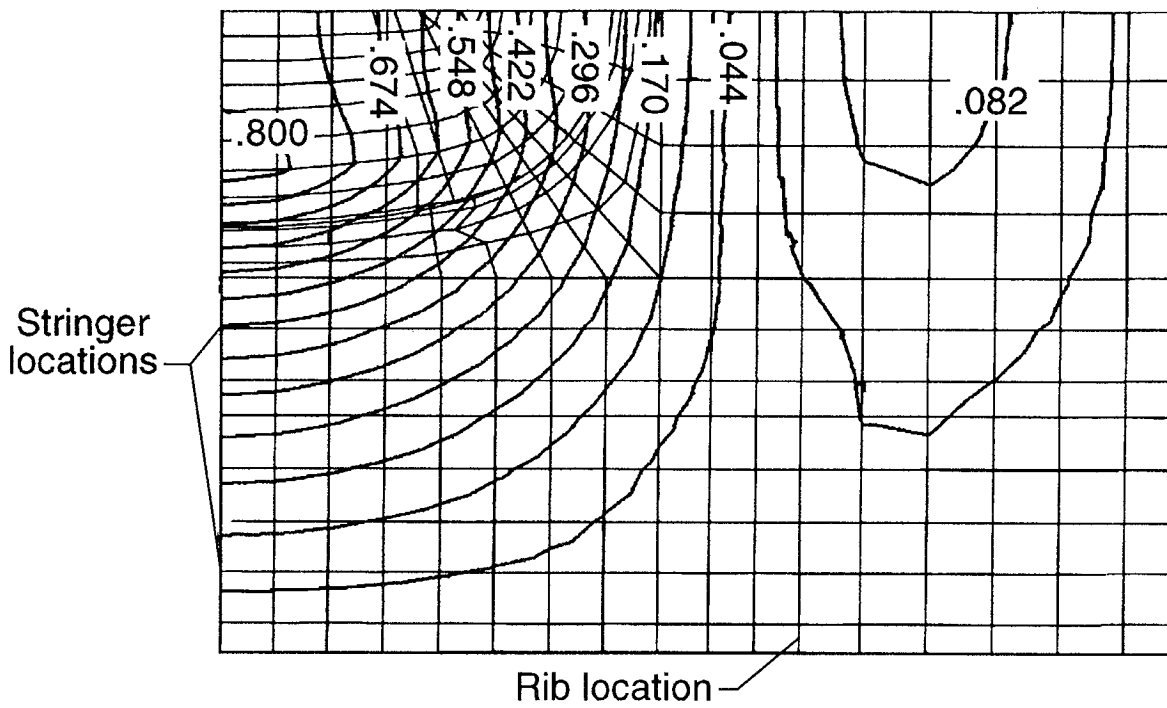
Figure 9. Contour plot of calculated out-of-plane deformations at P=688160 lb.
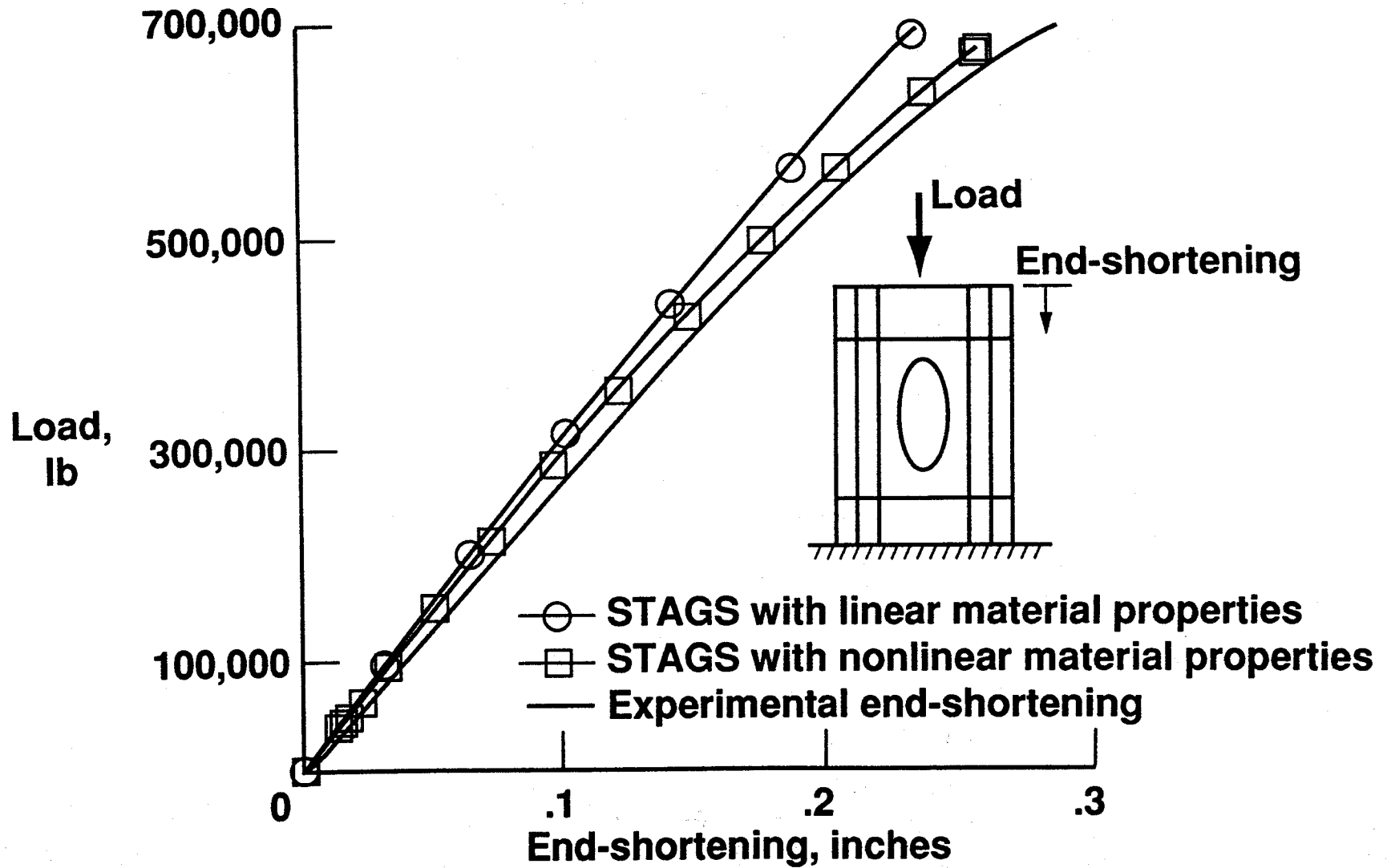
Figure 10.   Experimental and analytical end-shortening.

Applied load

Intercostal

— Undeformed
----- Deformed
→ DCDT

Lateral support frames

Aluminum plate

Rib

Intercostal

30
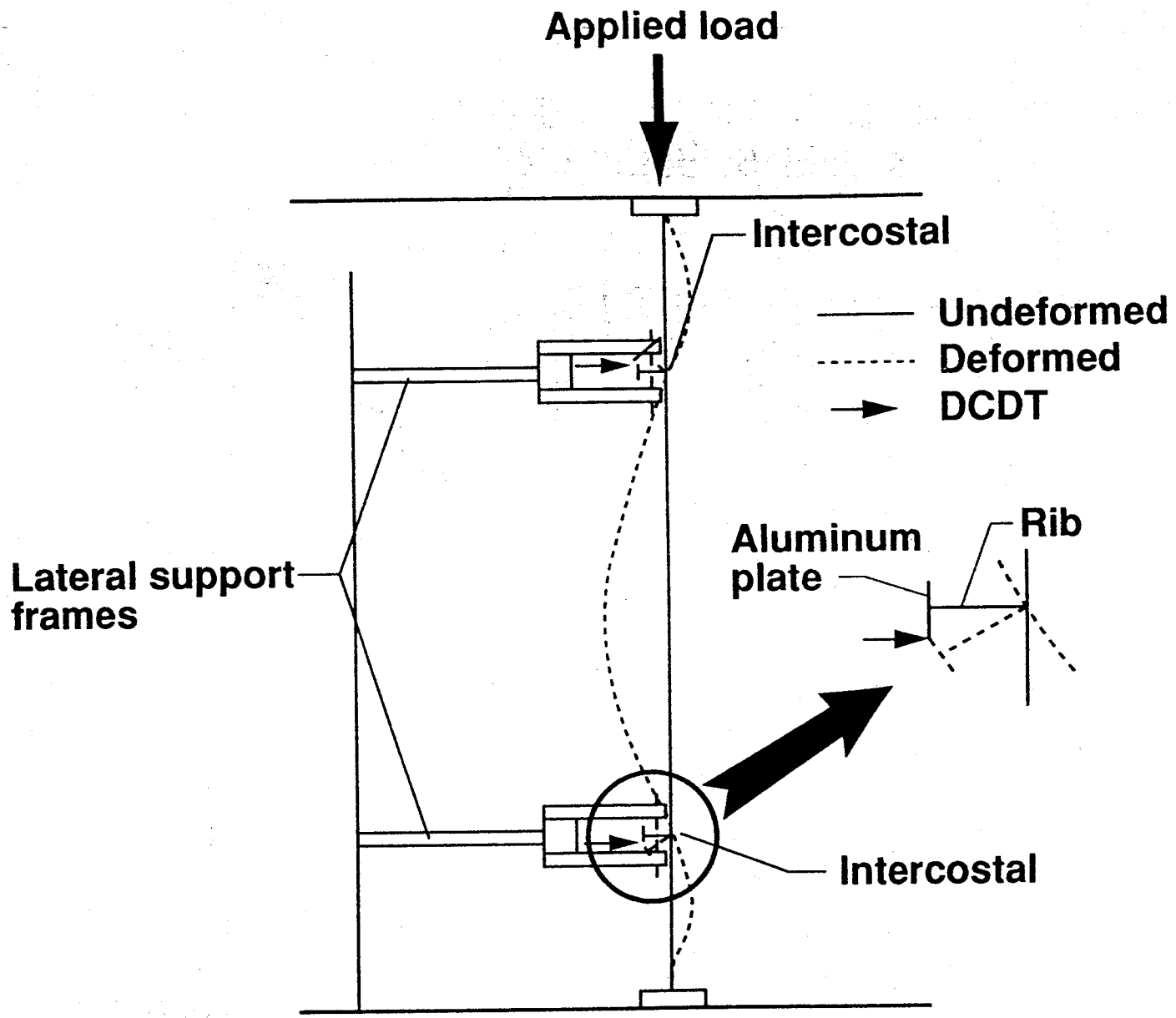
Figure 11. Sketch of side view of panel out-of-plane deformations showing rib rotation.

Figure 12.   Measurements of out-of-plane motion at the panel ribs.
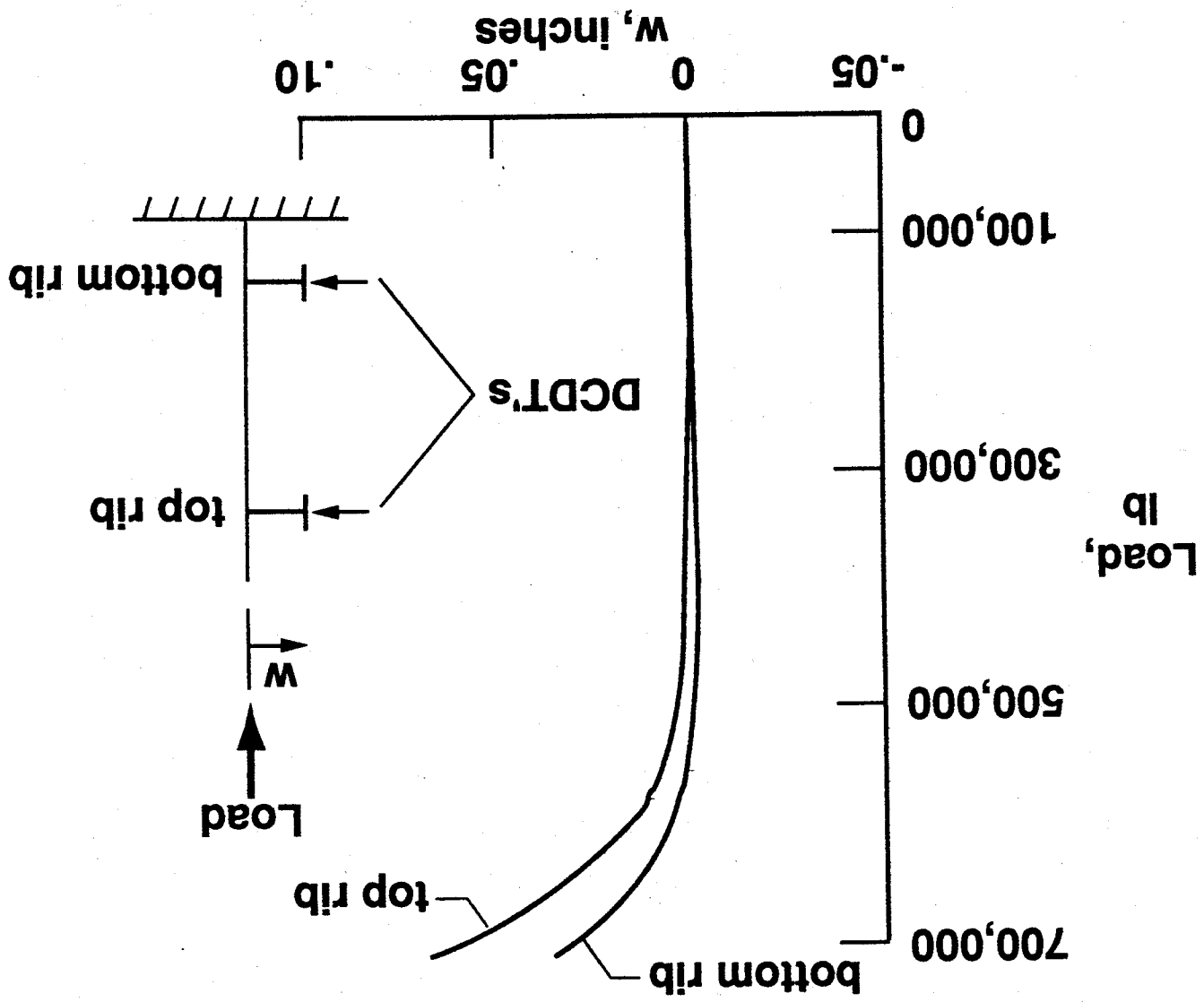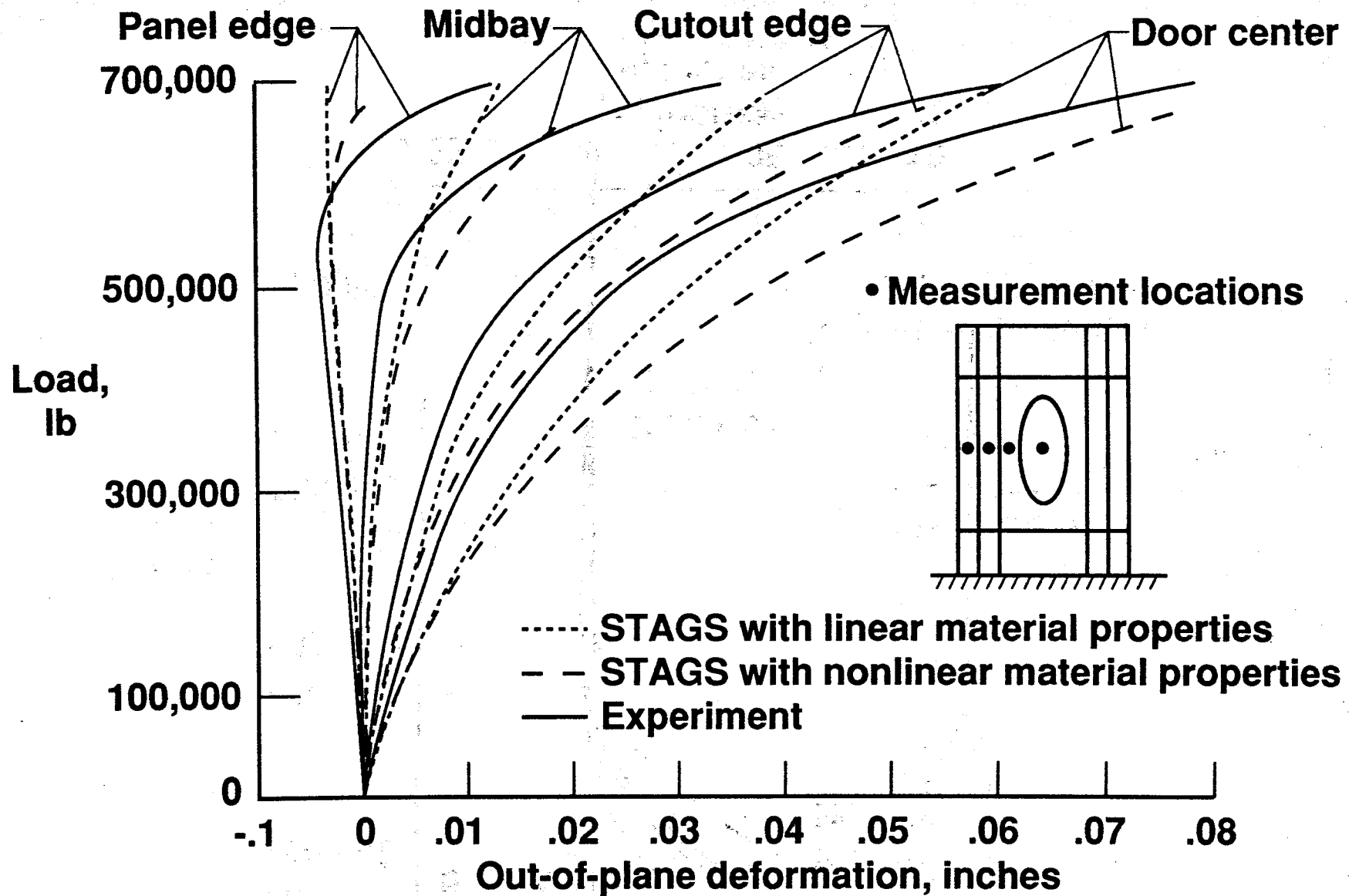
Figure 13. Experimental and analytical out-of-plane motion at panel centerline.
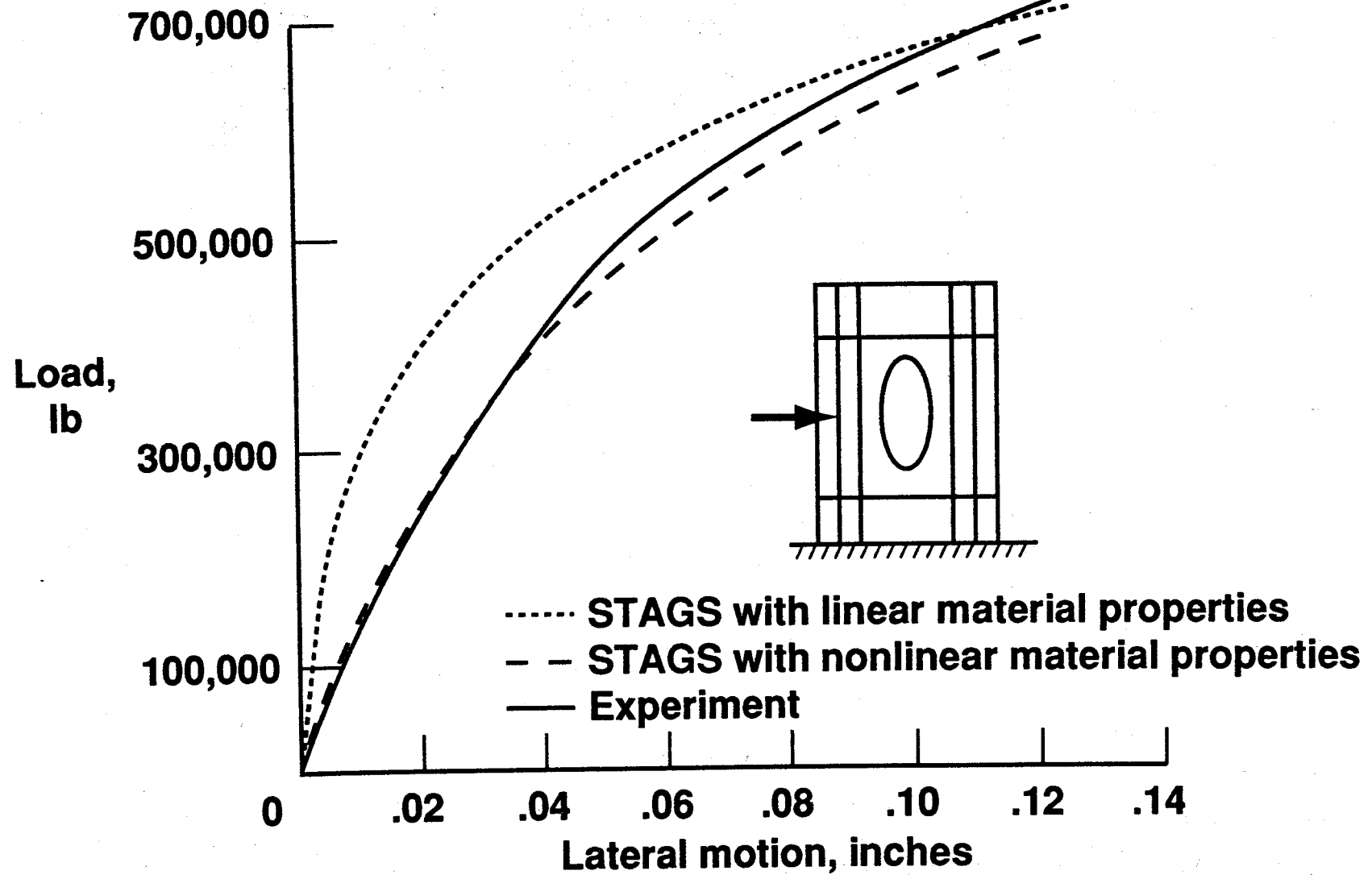
Figure 14.   Experimental and analytical rolling of outermost stringer.
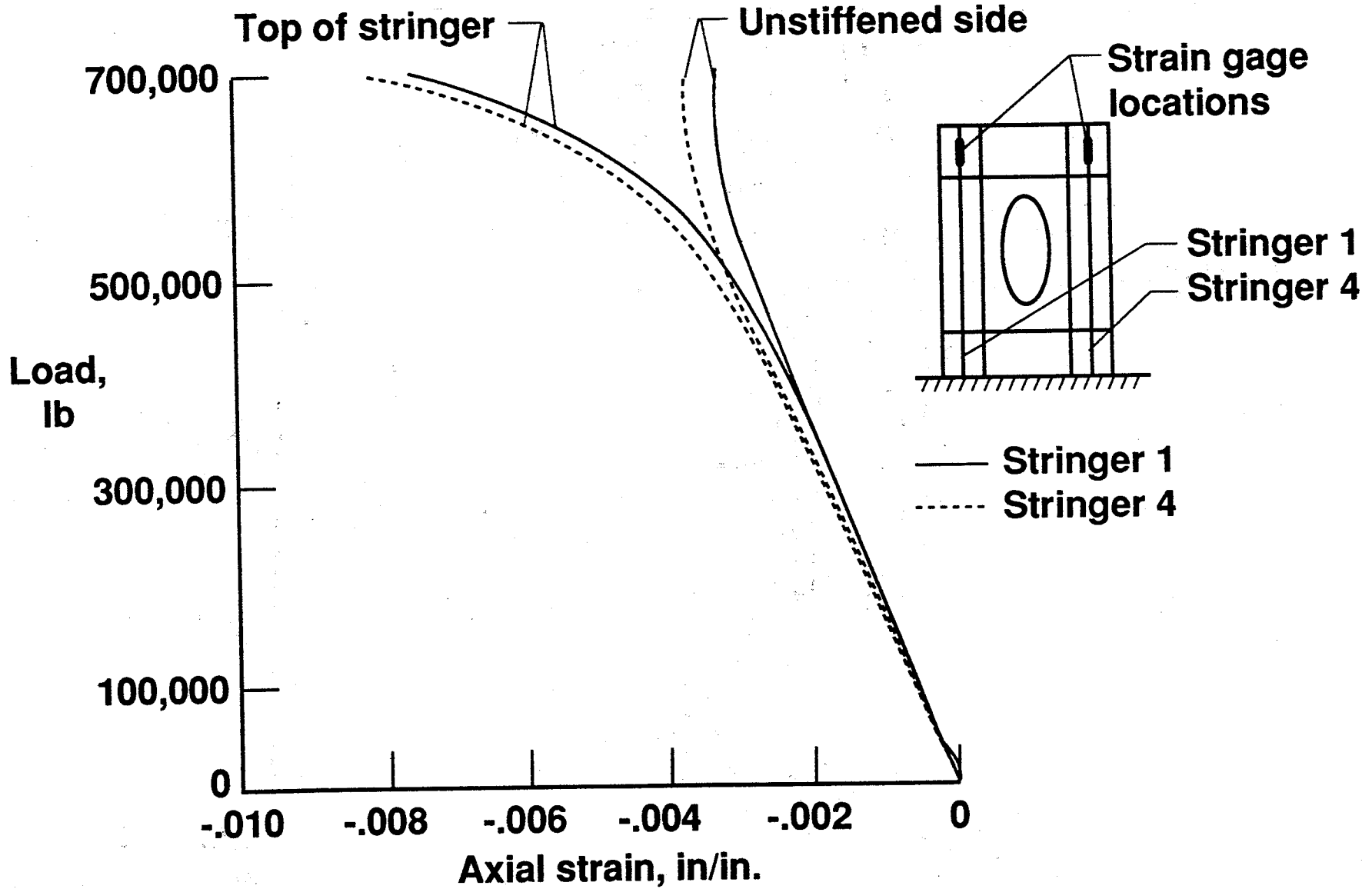
(a) Outermost stringers.
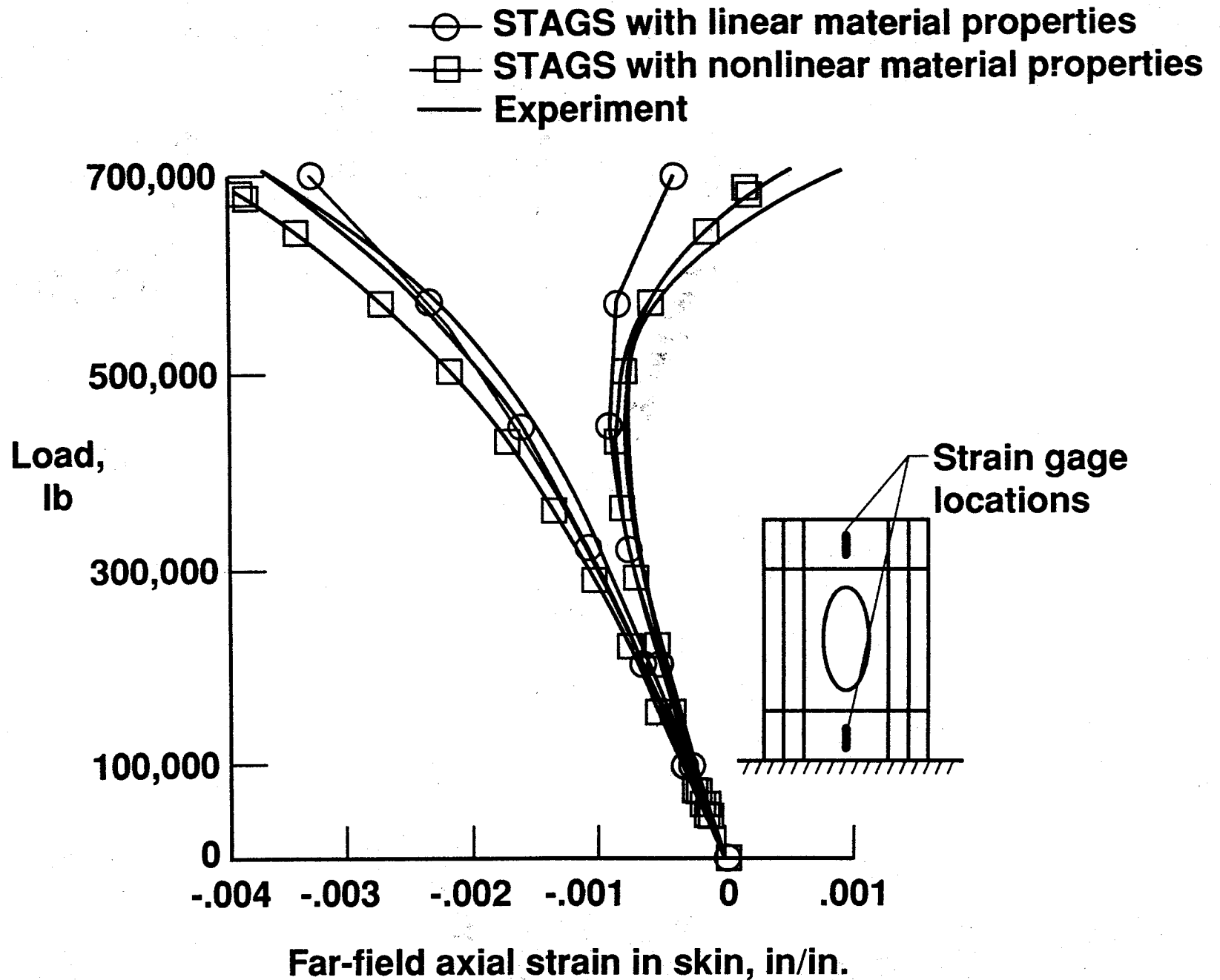
(b) Skin at lateral centerline.

Figure 15. Axial strain away from access door.
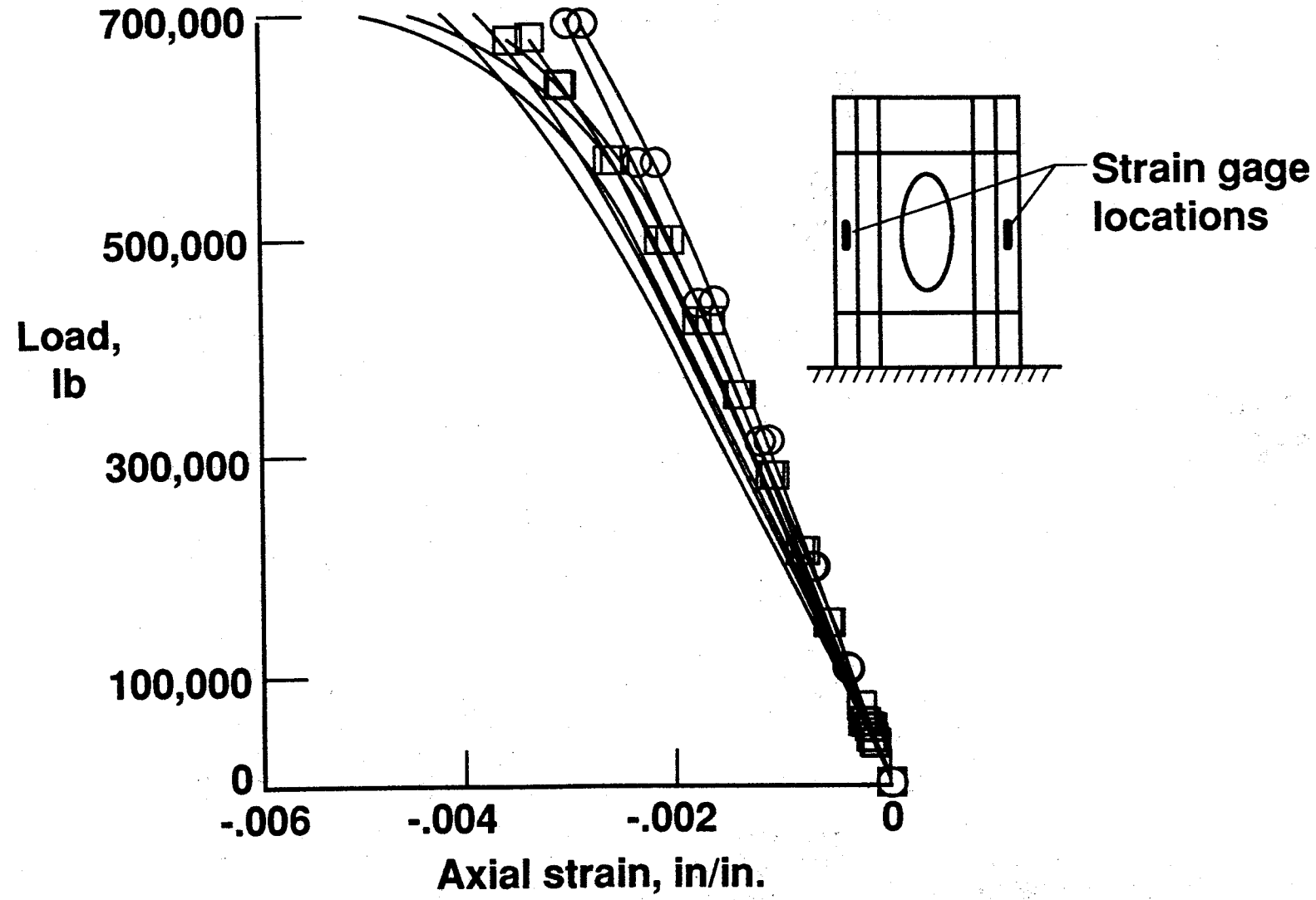
Figure 16. Axial strain in skin one inch from the panel edge.
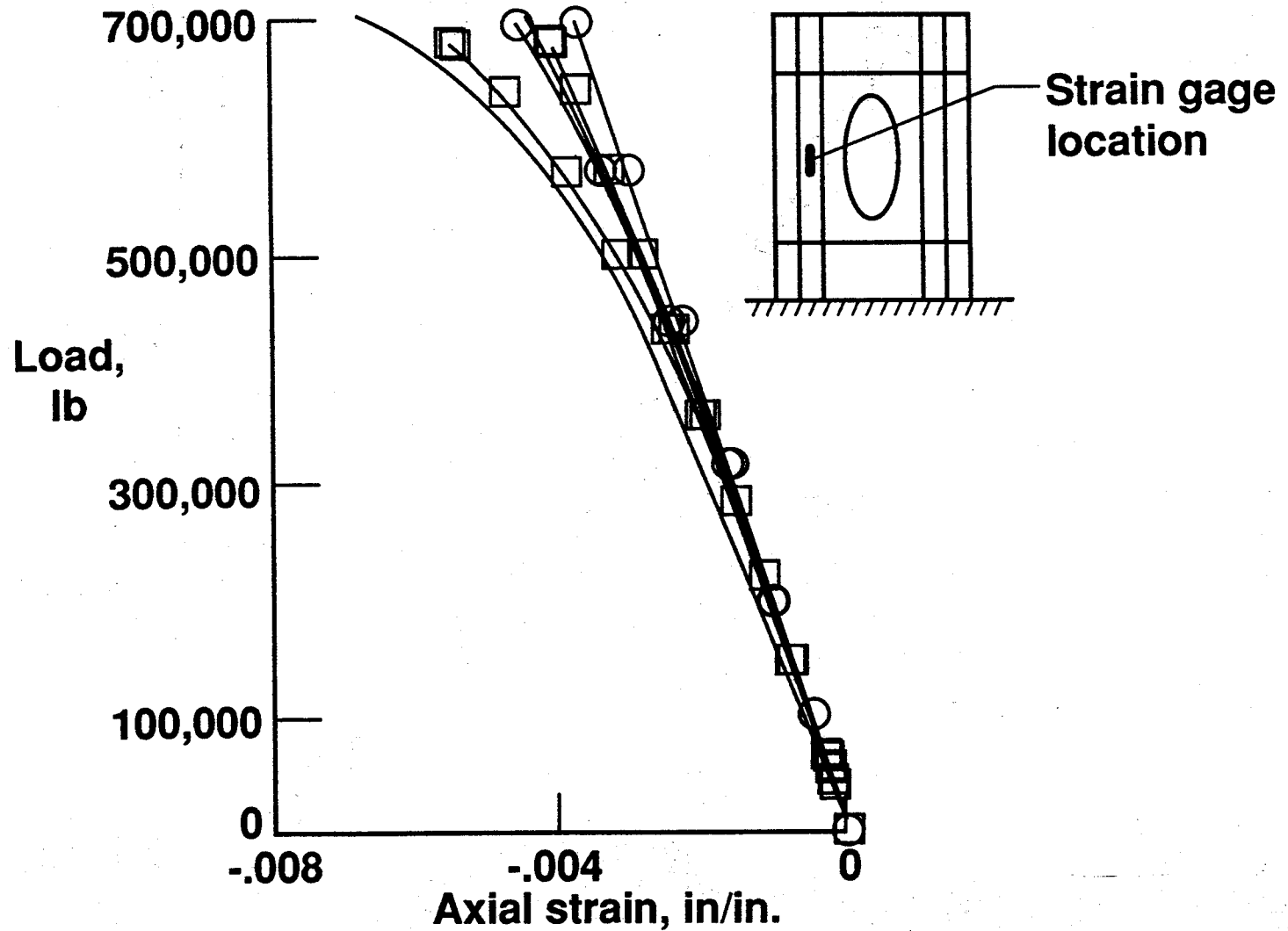
Figure 17.   Axial strain in panel skin between stringers.
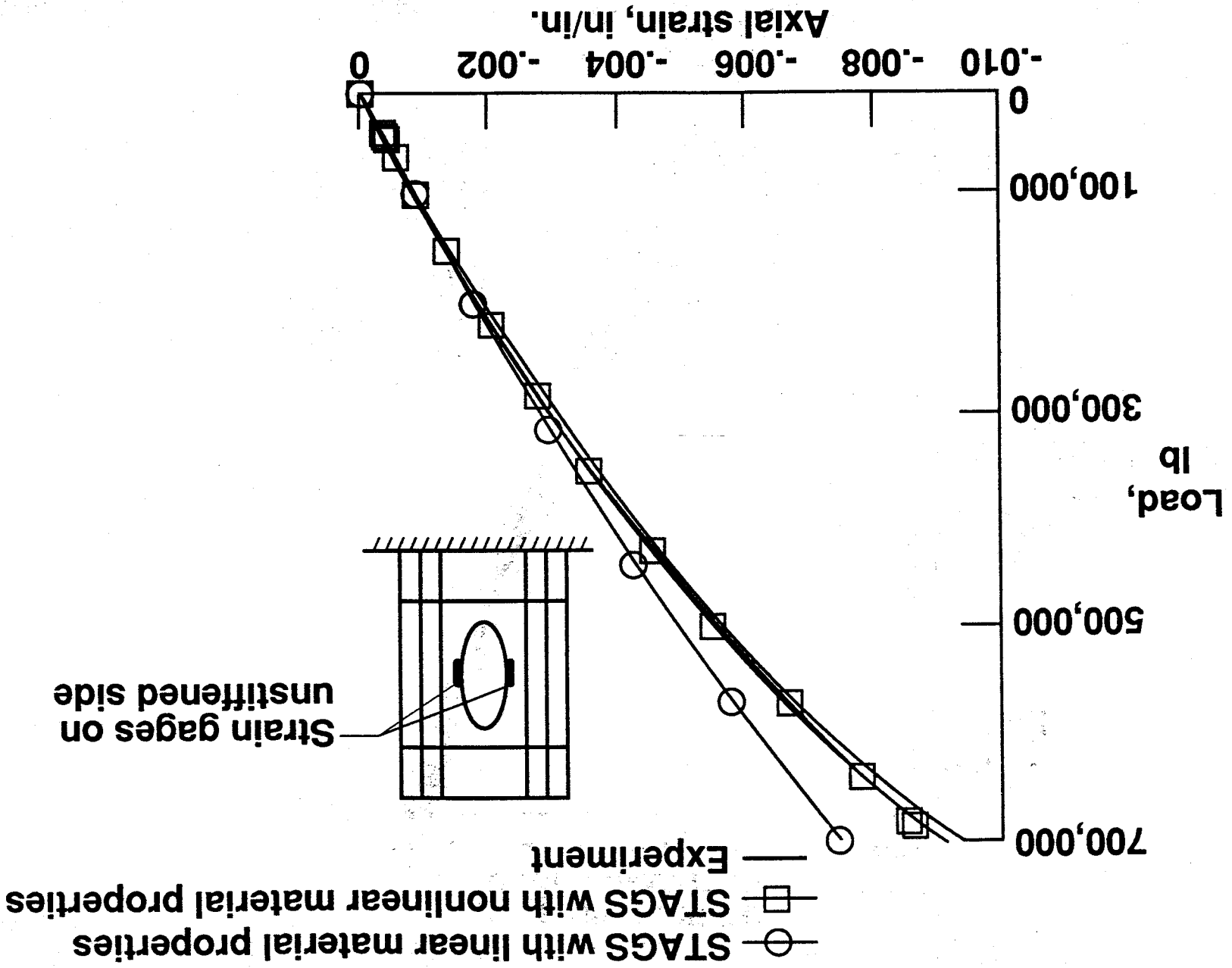
Figure 18. Axial strain in panel skin at edge of cutout.
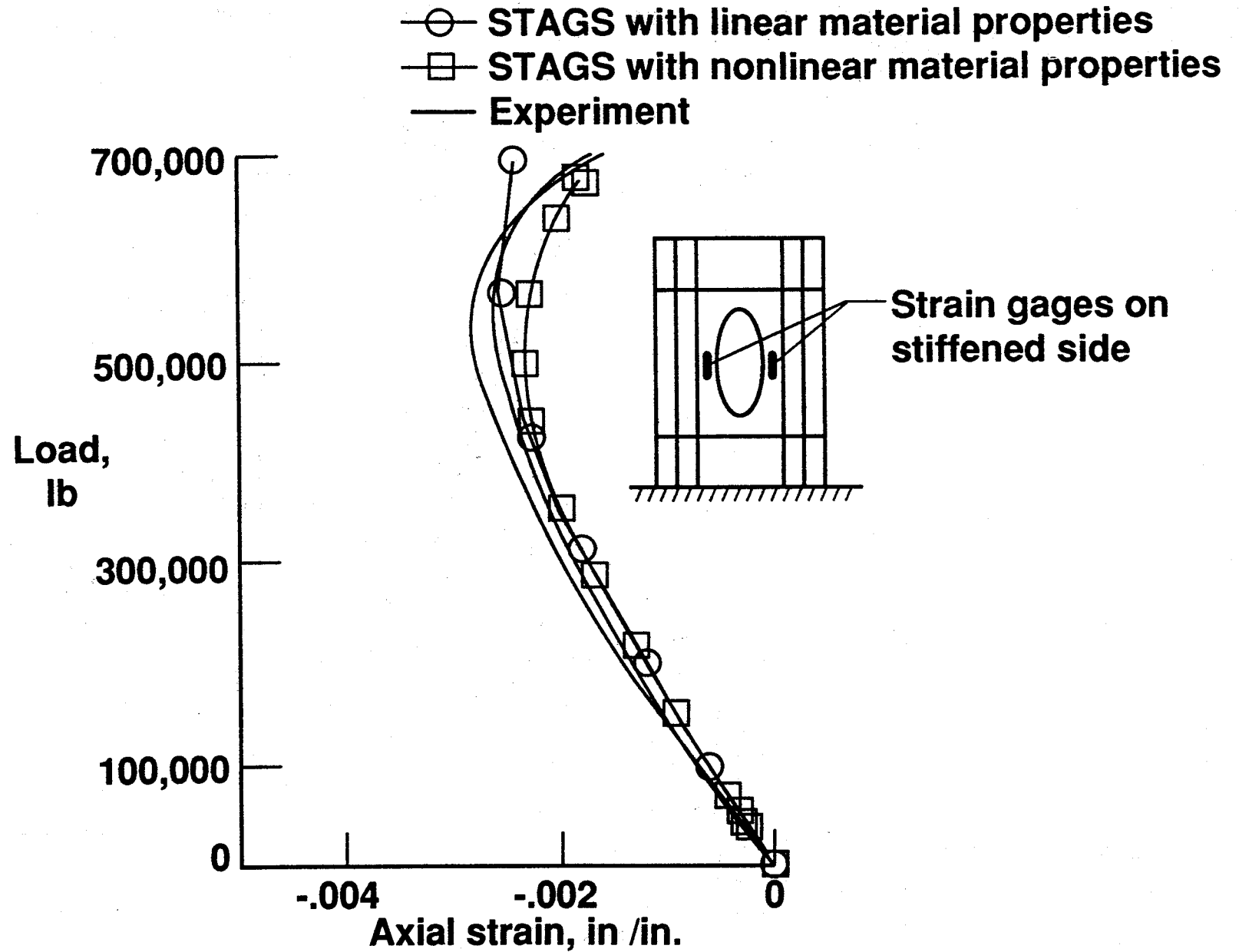
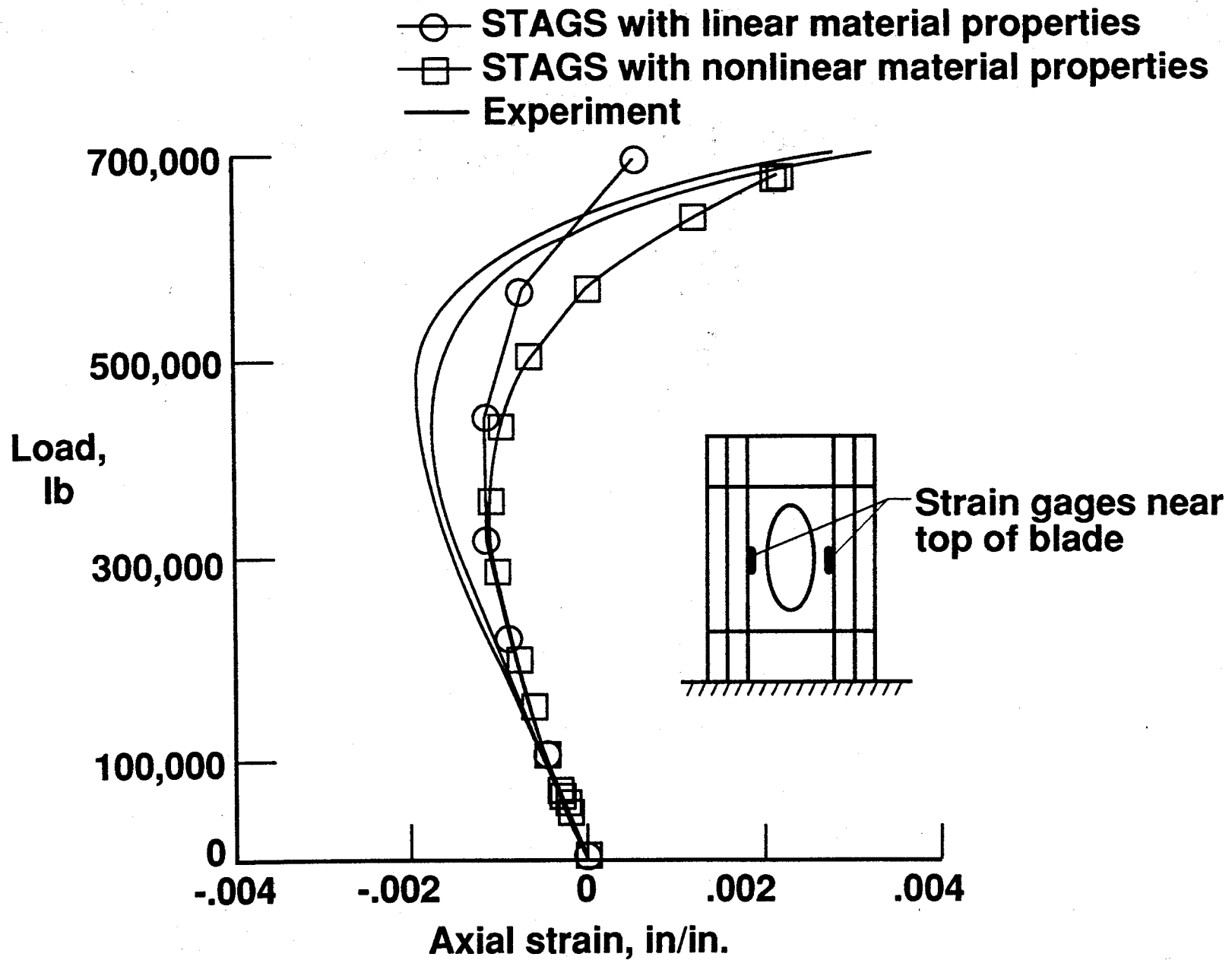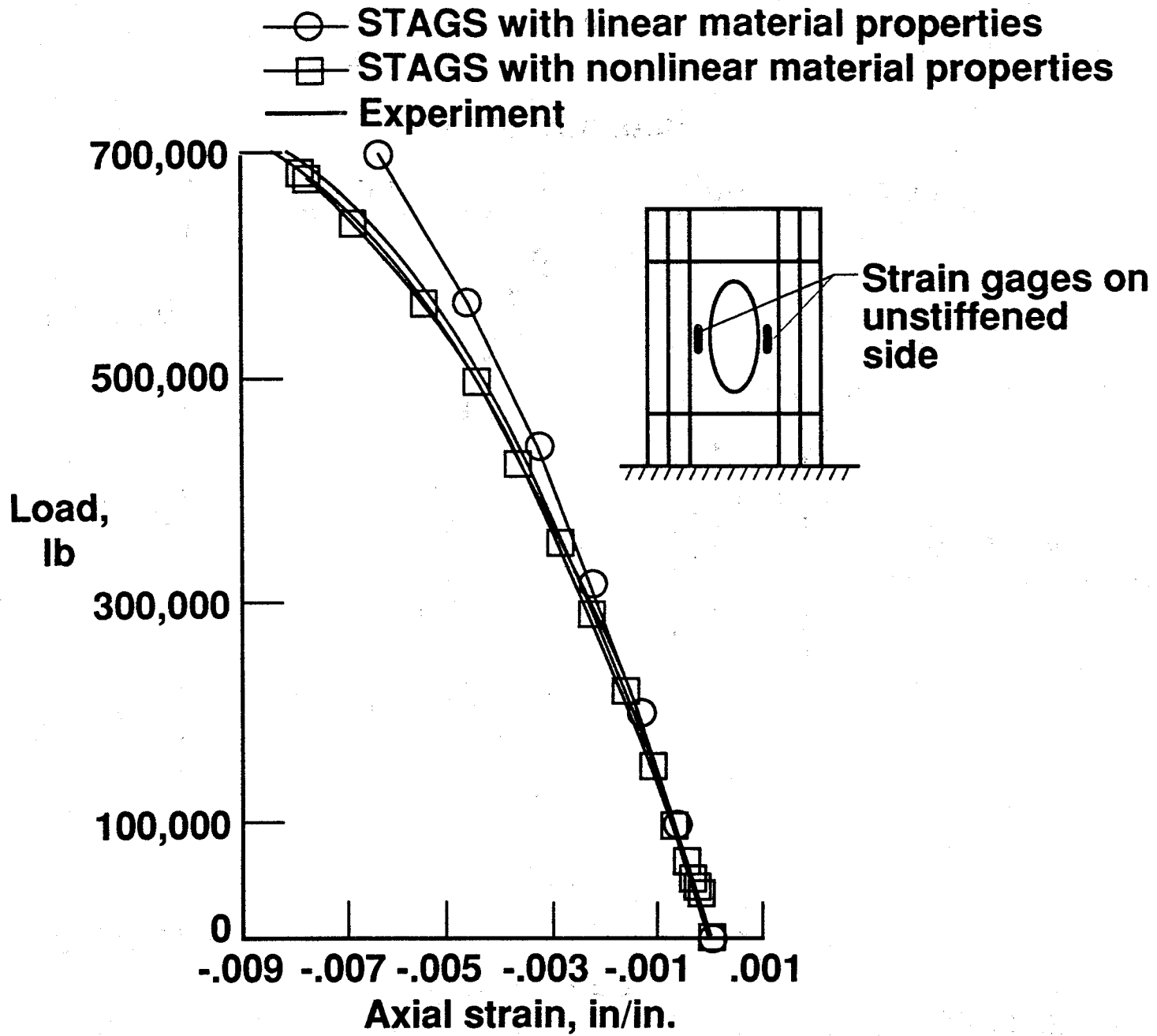Figure 19. Axial strain in land ring opposite to cutout edge in skin.
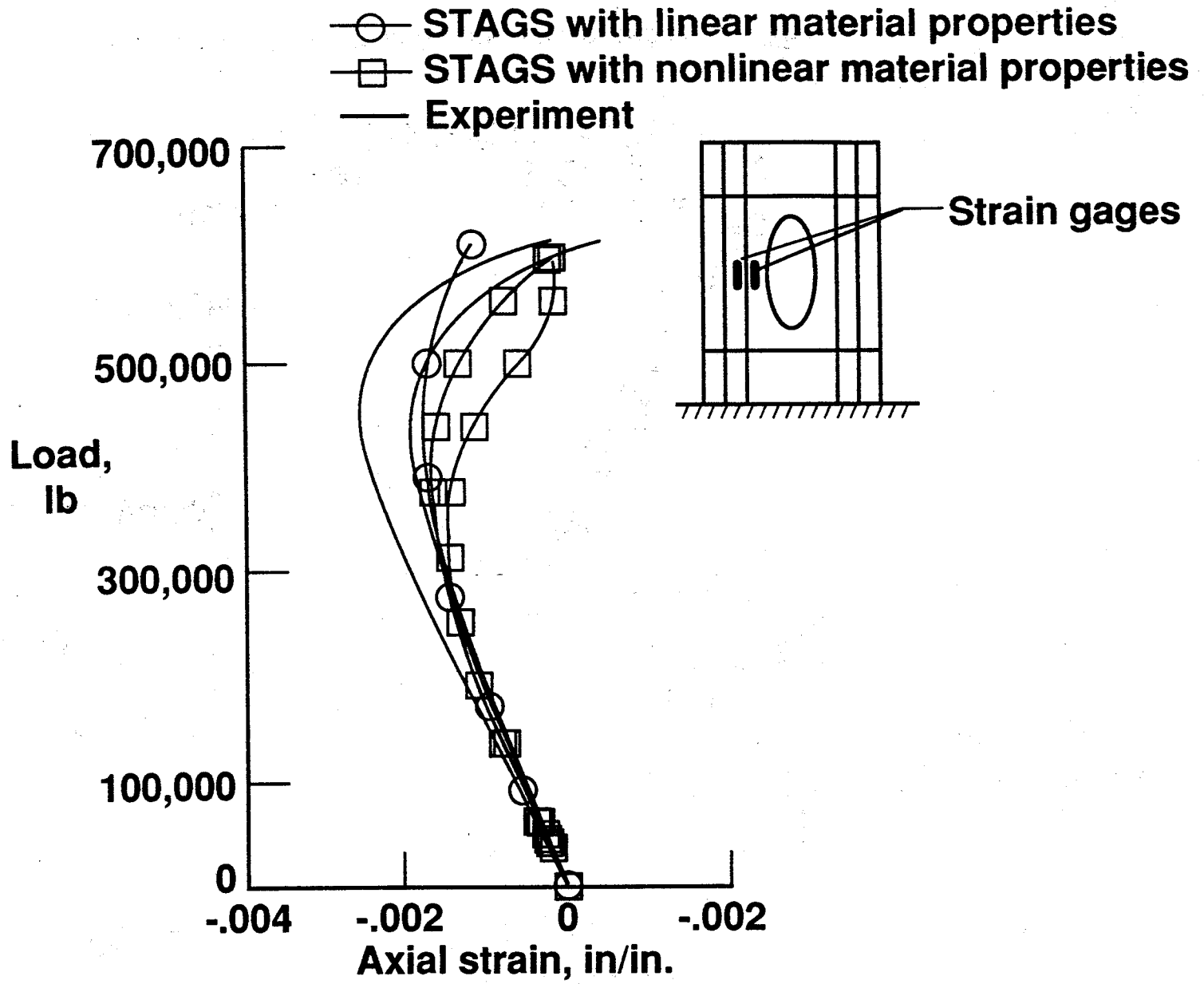
Figure 20.   Axial strain in centermost stringers.

(a) Axial strain in stringers.

21a

- ⊖ STAGS with linear material properties
- ⊟ STAGS with nonlinear material properties
- — Experiment

Strain gages on unstiffened side

(b) Axial strain in skin.
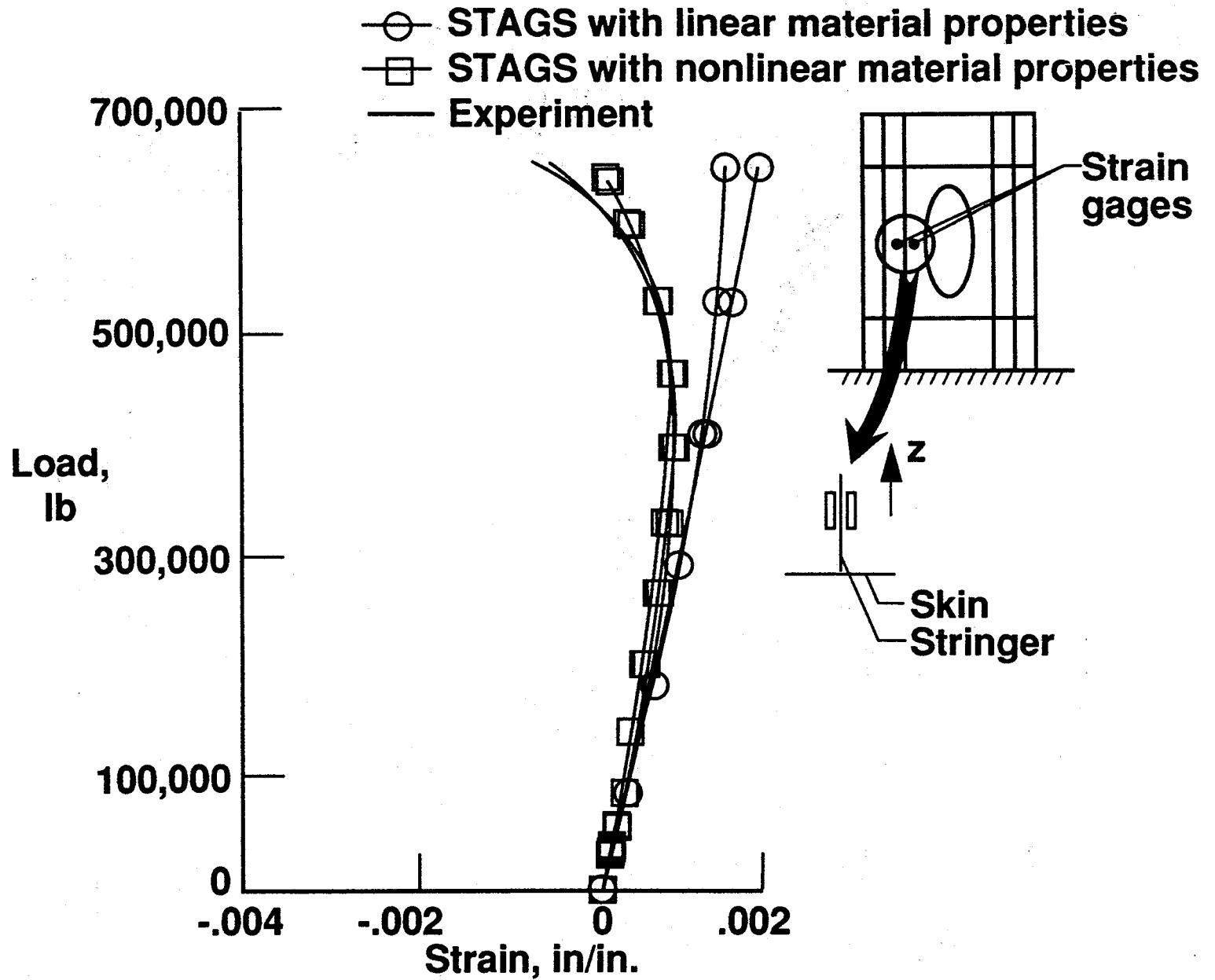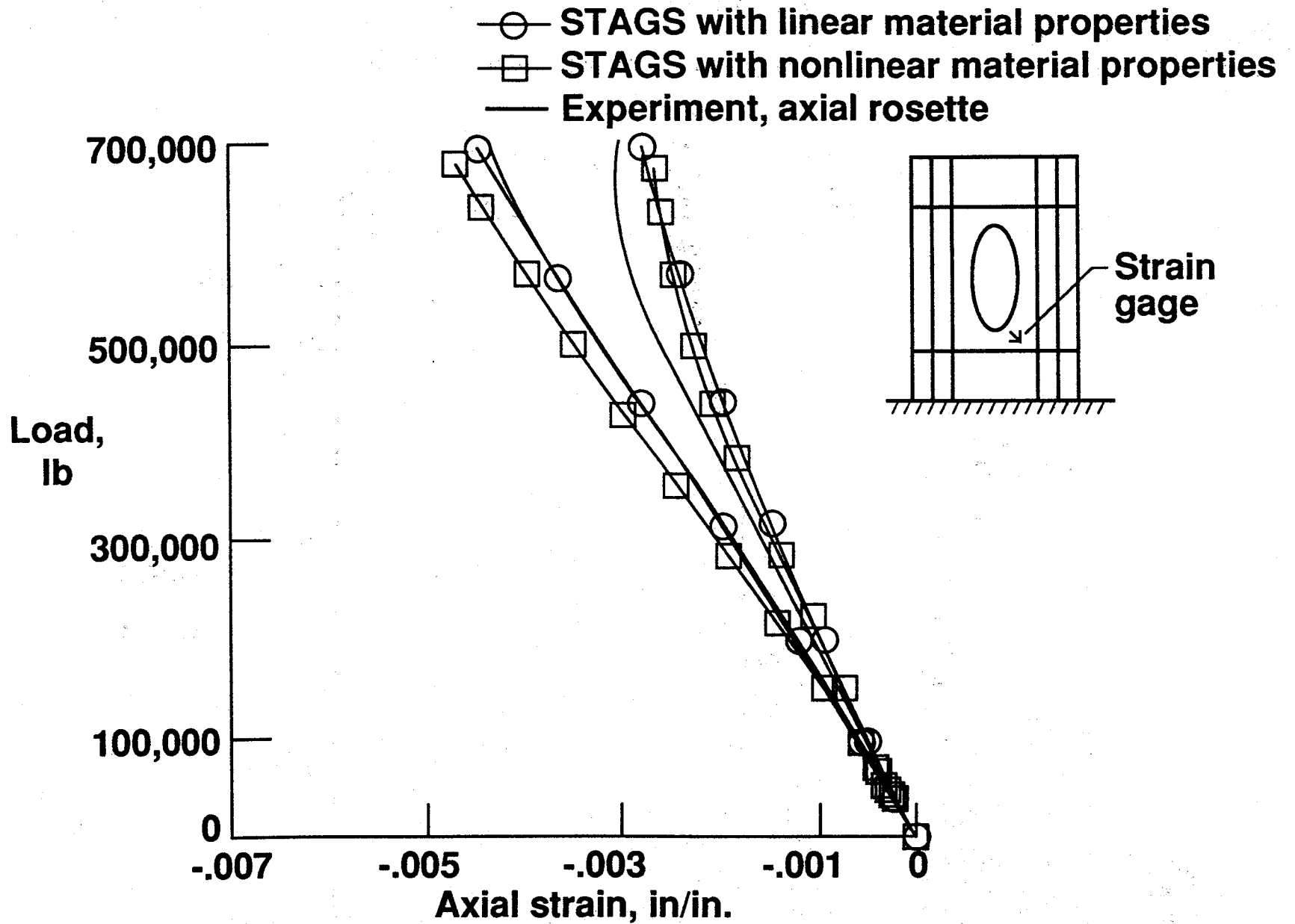
Figure 21. Axial strain in stringer and in skin.

Figure 22.   Strain due to rolling of stringer.

(a) Axial strain.

STAGS with linear material properties
STAGS with nonlinear material properties
Experiment, lateral rosette
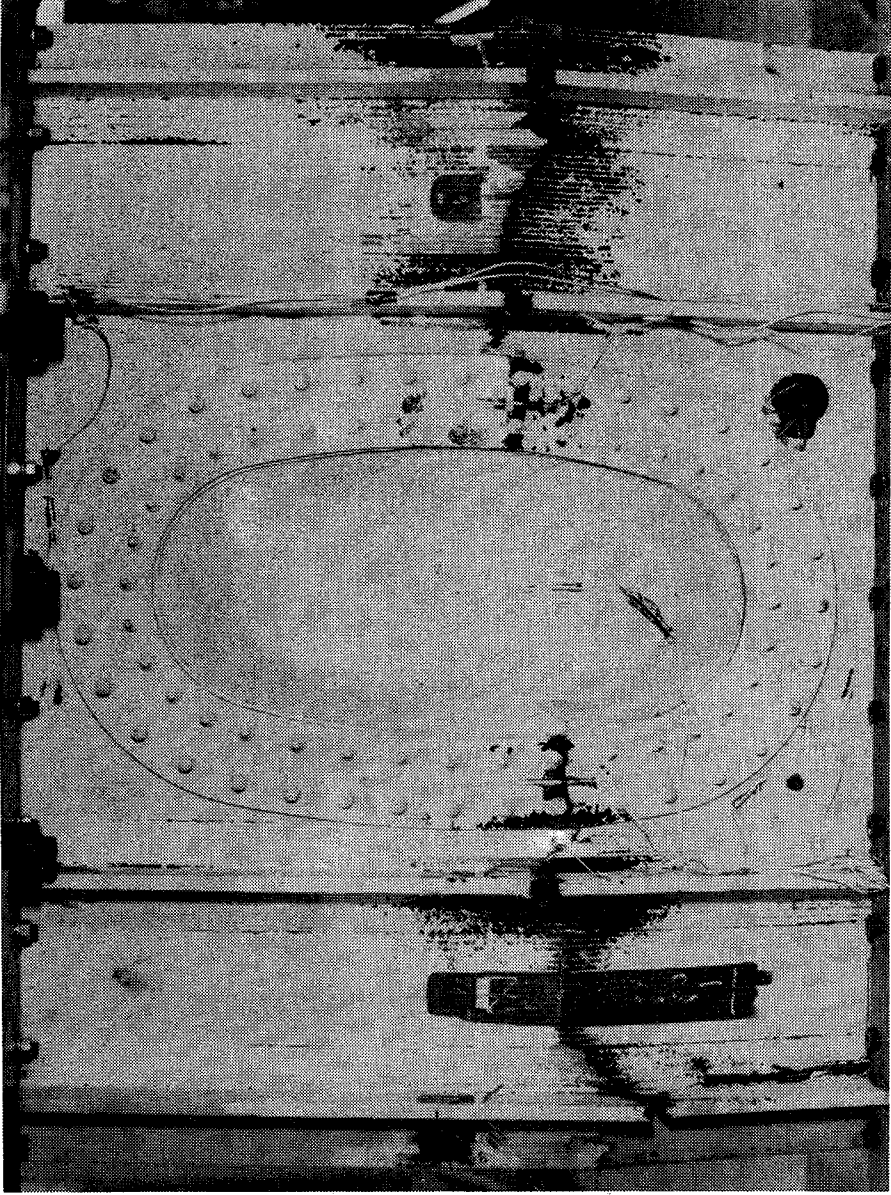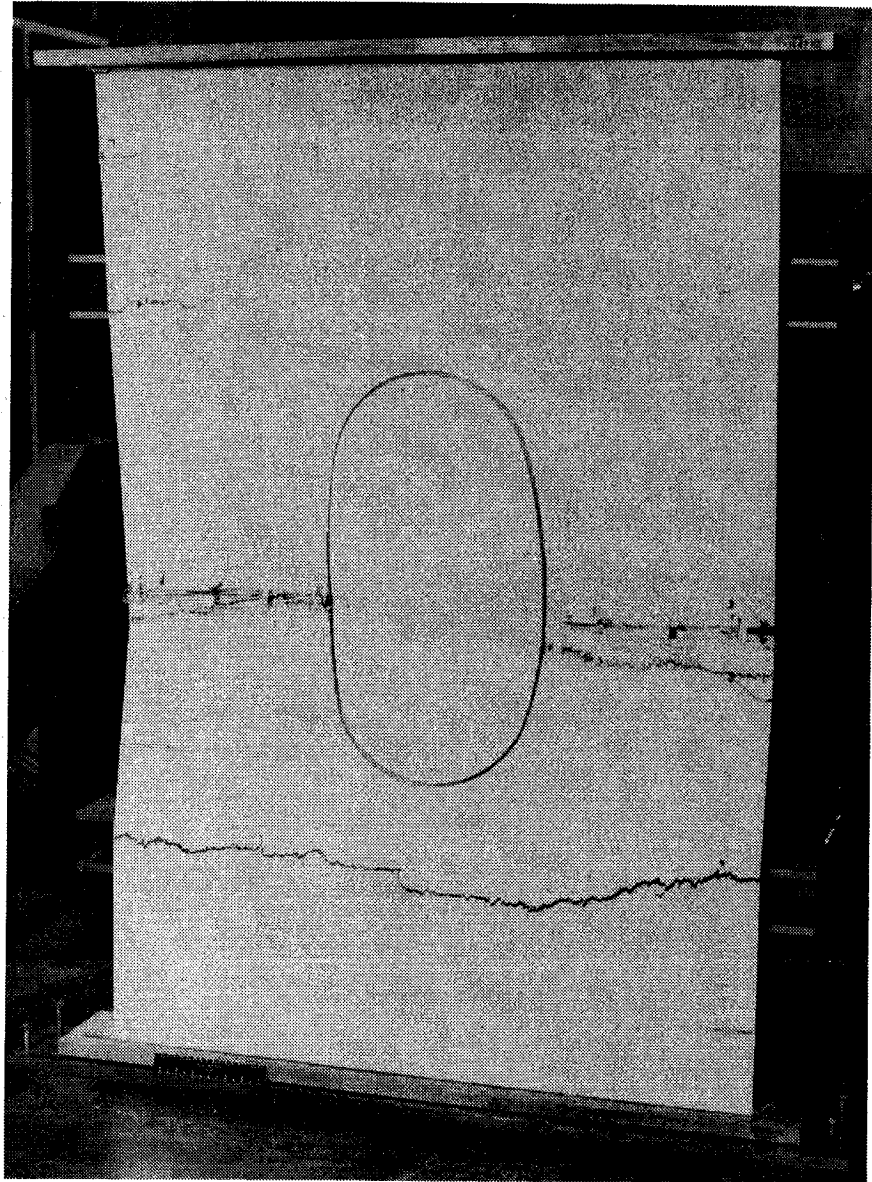
Strain gage
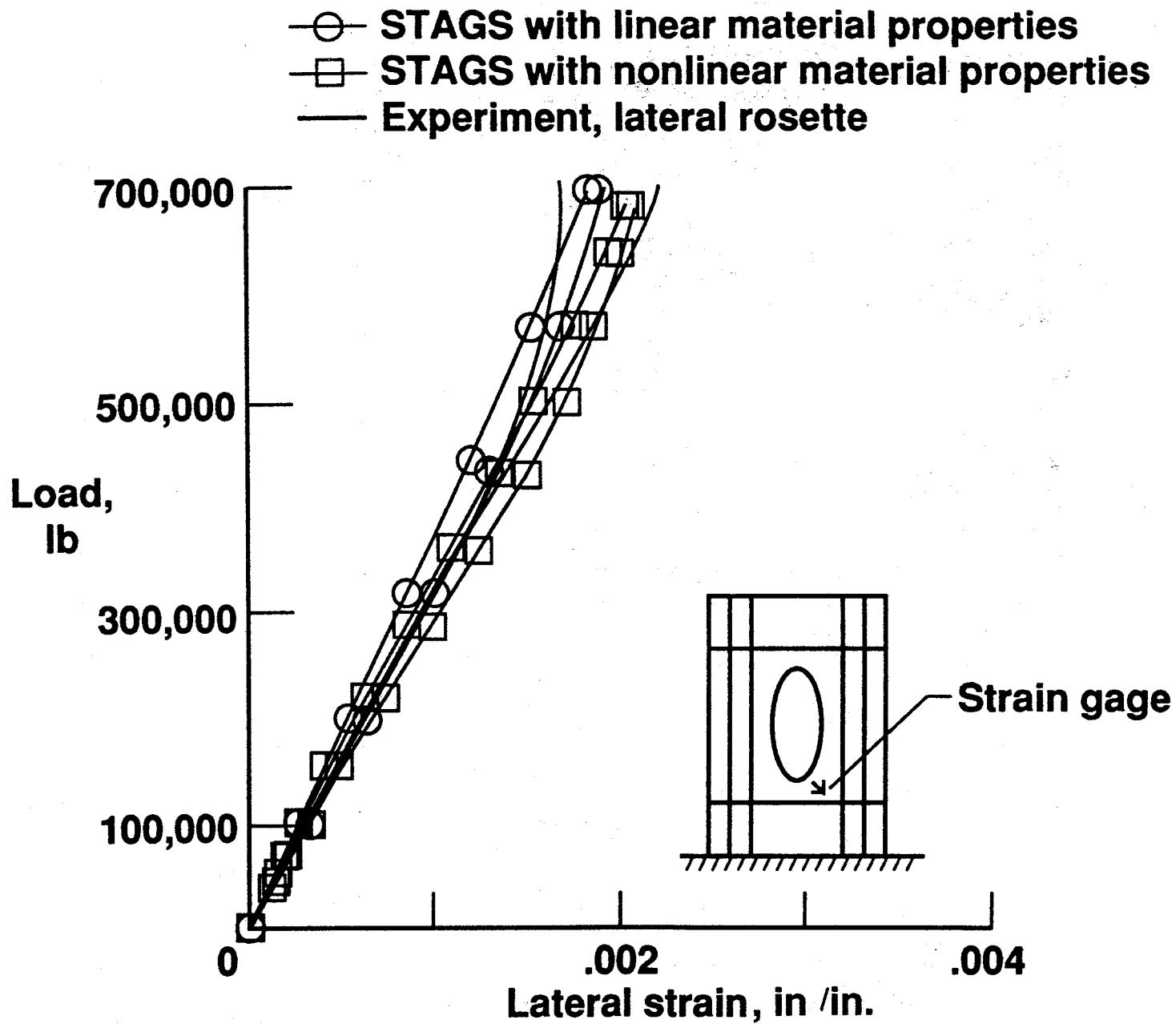
(b) Lateral strain.
Figure 23.   Strain in skin away from access door.

(a) Stiffened side.

46

(b) Unstiffened side.

.00314
.00220
.00127
.000339
-.000593
-.00153
-.00246
-.00339
-.00432
-.00525
-.00619
-.00712
-.00805
-.00898
-.00992
-.0108
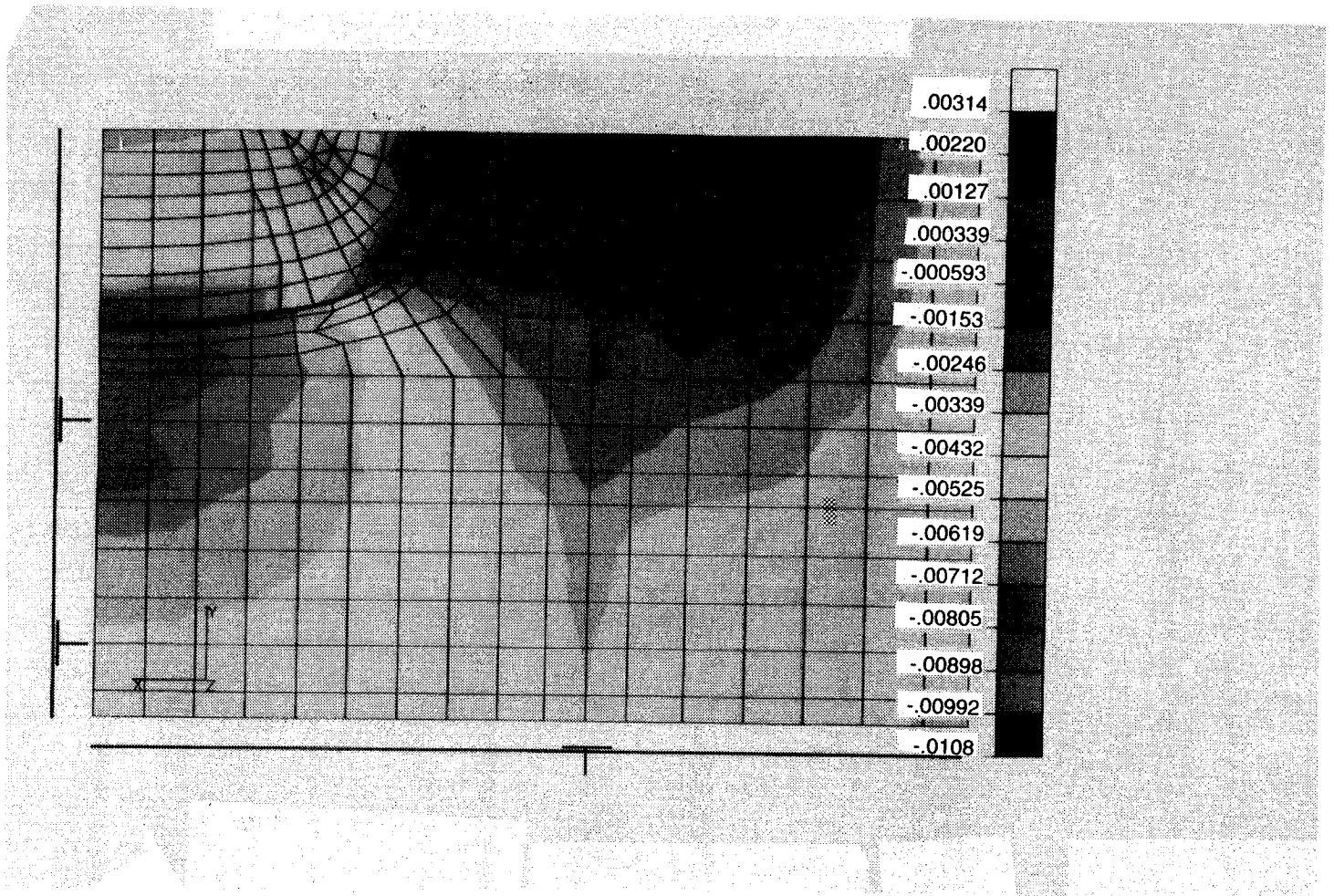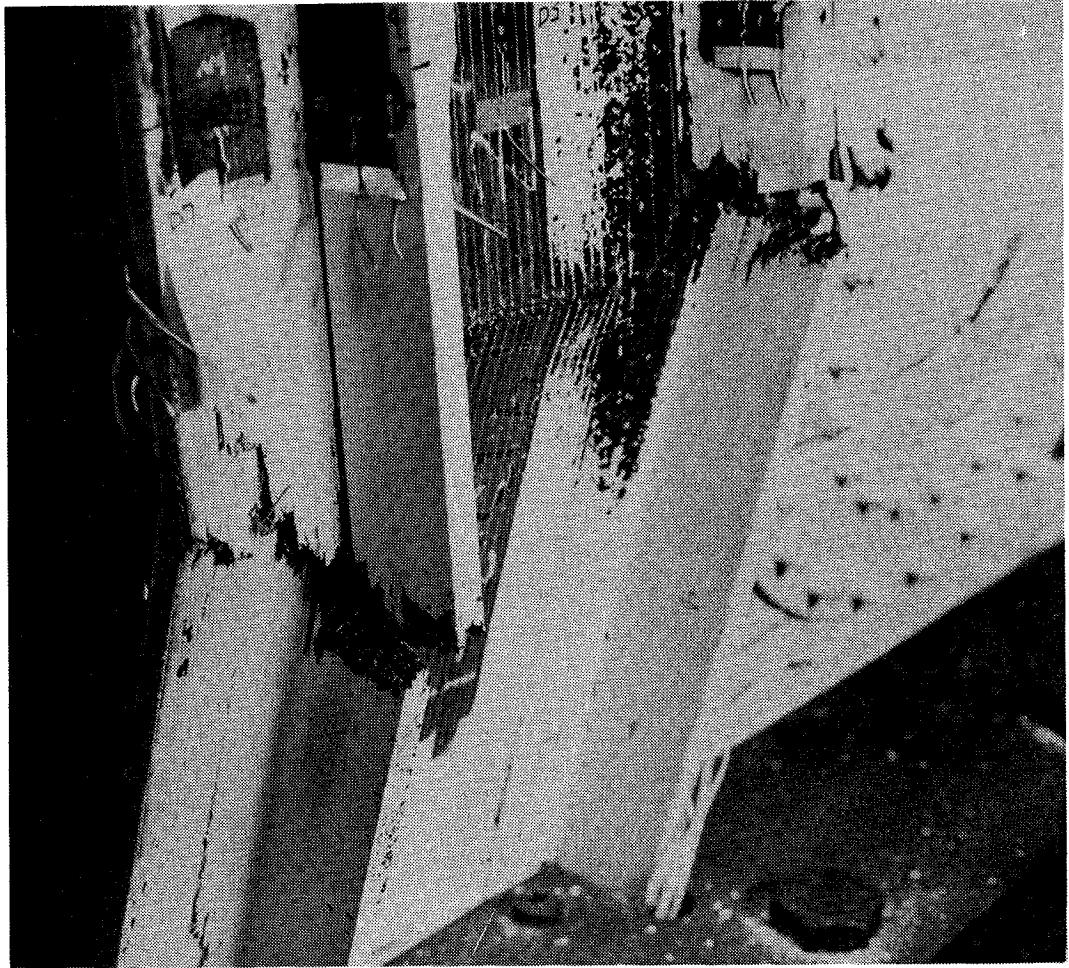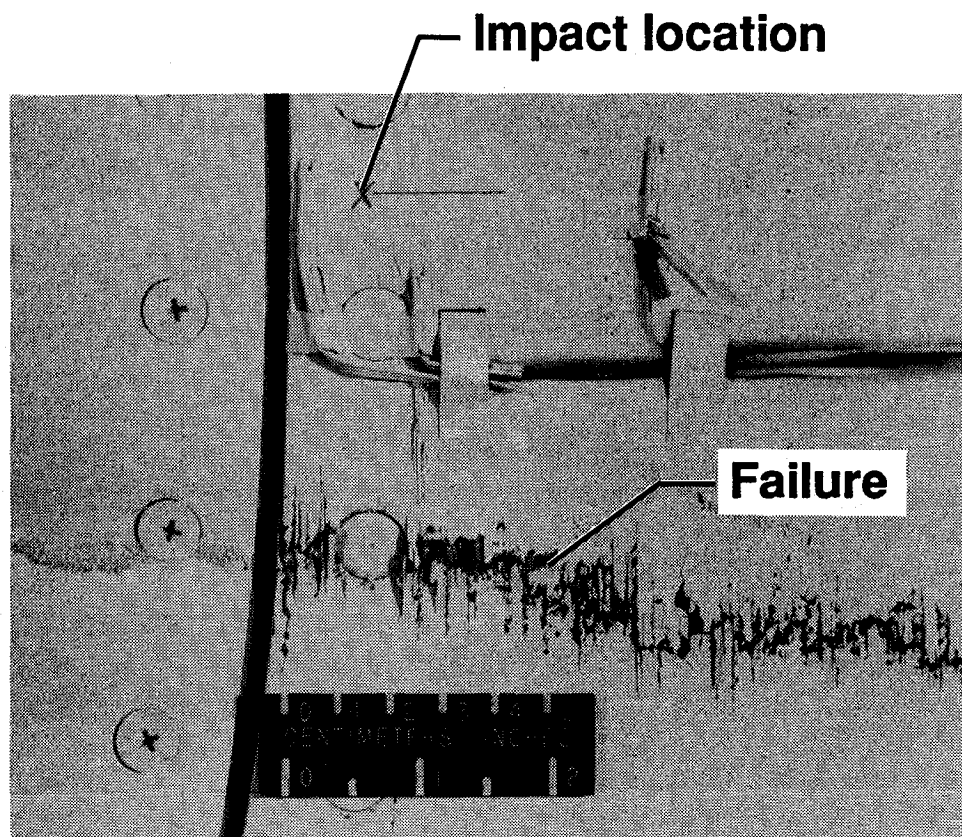
Figure 24.   Contour plot of axial strain at failure load.

(c) Broken stringers.
Figure 25.   Panel after failure.

Failure ——

—— **Impact location**

(a) Left side of door.

50

(b)   Right side of door.

Figure 26.   Failure and impact-damage locations on either side of access
door.

REPORT DOCUMENTATION PAGE		Form Approved OMB No. 0704-0188

Public reporting burden for this collection of information is estimated to average 1 hour per response, including the time for reviewing instructions, searching existing data sources, gathering and maintaining the data needed, and completing and reviewing the collection of information. Send comments regarding this burden estimate or any other aspect of this collection of information, including suggestions for reducing this burden, to Washington Headquarters Services, Directorate for Information Operations and Reports, 1215 Jefferson Davis Highway, Suite 1204, Arlington, VA 22202-4302, and to the Office of Management and Budget, Paperwork Reduction Project (0704-0188), Washington, DC 20503.

1. AGENCY USE ONLY (Leave blank)	2. REPORT DATE March 1994	3. REPORT TYPE AND DATES COVERED Technical Memorandum

4. TITLE AND SUBTITLE Test and Analysis of a Stitched RFI Graphite-Epoxy Panel with a Fuel Access Door	5. FUNDING NUMBERS WU 510-02-12-01

6. AUTHOR(S)

Dawn C. Jegley and W. Allen Waters, Jr.

7. PERFORMING ORGANIZATION NAME(S) AND ADDRESS(ES) NASA Langley Research Center Hampton, VA 23681-0001	8. PERFORMING ORGANIZATION REPORT NUMBER

9. SPONSORING / MONITORING AGENCY NAME(S) AND ADDRESS(ES) National Aeronautics and Space Administration Washington, DC 20546-0001	10. SPONSORING / MONITORING AGENCY REPORT NUMBER NASA TM 108992

11. SUPPLEMENTARY NOTES

12a. DISTRIBUTION / AVAILABILITY STATEMENT Unclassified - Unlimited Subject Category - 24	12b. DISTRIBUTION CODE

13. ABSTRACT (Maximum 200 words)

A stitched RFI graphite-epoxy panel with a fuel access door was analyzed using a finite element analysis and loaded to failure in compression. The panel was initially 56-inches long and 36.75-inches wide and the oval access door was 18-inches long and 15-inches wide. The panel was impact damaged with impact energy of 100 ft-lb prior to compressive loading; however, no impact damage was detectable visually or by A-scan. The panel carried a failure load of 695,000 lb and global failure strain of .00494 in/in. Analysis indicated the panel would fail due to collapse at a load of 688,100 lb. The test data indicate that the maximum strain in a region near the access door was .0096 in/in and analysis indicates a local surface strain of .010 in/in at the panel's failure load. The panel did not fail through the impact damage, but instead failed through bolt holes for attachment of the access door in a region of high strain.

14. SUBJECT TERMS stitching, resin fusion injection, low-speed impact damage, graphite-epoxy			15. NUMBER OF PAGES 52
			16. PRICE CODE A04

17. SECURITY CLASSIFICATION OF REPORT Unclassified	18. SECURITY CLASSIFICATION OF THIS PAGE Unclassified	19. SECURITY CLASSIFICATION OF ABSTRACT Unclassified	20. LIMITATION OF ABSTRACT